



Synergistic effects of electrical and chemical cues with biodegradable scaffolds for large peripheral nerve defect regeneration

Rosalie Bordett^a , Sama Abdulmalik^b , Allen Zennifer^b , Suranji Wijekoon^b,
Sai Sadhananth Srinivasan^b , Ergin Coskun^a , Yeshavanth Kumar Banasavadi Siddegowda^c,
Xiaojun Yu^d , Sangamesh G. Kumbar^{a,b,*} 

^a Department of Orthopedic Surgery, University of Connecticut Health Center, 263 Farmington Avenue, Farmington, CT, 06030-4037, USA

^b Department of Growth and Development, College of Dentistry, University of Nebraska Medical Center, Joseph D. & Millie E. Williams Science Hall, 525 S 42nd St, Omaha, NE, 68105, USA

^c Surgical Neurology Branch, National Institute of Neurological Disorders and Stroke, National Institutes of Health, Bethesda, MD, USA

^d Department of Biomedical Engineering, Stevens Institute of Technology, 1 Castle Point on Hudson, Hoboken, New Jersey, USA

ARTICLE INFO

Keywords:

Peripheral nerve regeneration
Ionic conductive nerve conduits
4-Aminopyridine (4-AP)
Transcutaneous electrical stimulation
Schwann cell proliferation
Neurotrophic factors
Sciatic nerve injury repair

ABSTRACT

Large-gap peripheral nerve injuries (PNI) are often treated with autografts, allografts, or synthetic grafts to facilitate nerve regeneration, but these options are often limited in their availability or functionality. To address these issues, we developed ionically conductive (IC) nerve guidance conduits (NGCs) of sufficient biodegradability, mechanical strength, and bioactivity to support large-gap nerve regeneration. These chitosan-based NGCs release 4-aminopyridine (4-AP) from embedded halloysite nanotubes, and the NGC's IC properties enable transcutaneous electrical stimulation (ES) without invasive electrodes. *In vitro*, we found scaffolds with ES+4-AP synergistically enhanced Schwann cell adhesion, proliferation, and neurotrophin secretion, significantly improving axonal growth and neurite extension. *In vivo*, these scaffolds in large-gap PNI boosted neurotrophin levels, myelination, nerve function, and muscle weight while promoting angiogenesis and reducing fibrosis. Upregulated Trk receptors and PI3K/Akt and MAPK pathway highlight the regenerative potential. This study advances understanding of ES-mediated regeneration and supports innovative strategies for nerve and musculoskeletal repair.

1. Introduction

Each year, over half a million Americans suffer from peripheral nerve injuries (PNI), requiring surgical treatments that amount to approximately \$2 billion in healthcare costs [1]. Despite treatment, many patients still experience pain and reduced functionality. Severe PNI, typically involving gaps larger than 4 cm, cannot regenerate without surgical intervention. The primary treatments include autografts and allografts, but these are often limited by availability and associated with issues like immunosuppression, donor site morbidity, scarring, neuroma formation, and sensory loss [2]. Tissue engineering (TE) approaches, which involve scaffolds, cells, and growth factors, offer potential alternatives to biological grafts. However, limitations such as gap size, biocompatibility, and insufficient stimulation of nerve regeneration

restrict their widespread use [3]. Ineffective repair can result in significant sensory or motor function loss [2], with more severe injuries linked to slower recovery, highlighting the need for improved treatments. Chemical [4] and electrical stimulation [5] have shown the ability to enhance endogenous nerve regeneration in less severe PNI and may also have the potential for treating severe cases. Thus, combining the design flexibility and on-demand availability of engineered synthetic and biological scaffolds with robust and consistent stimulation of endogenous nerve repair mechanisms will address current treatment limitations and ultimately enhance functional outcomes of large-gap PNI repair in humans.

Peripheral nerve injuries vary in severity, and different models are used to study nerve regeneration and test treatments. Injuries that can regenerate spontaneously retain some axonal continuity at the lesion

Peer review under the responsibility of editorial board of Bioactive Materials.

* Corresponding author. Department of Growth and Development, College of Dentistry, University of Nebraska Medical Center, Joseph D. & Millie E. Williams Science Hall, 525 S 42nd St, Room No 4.0.011, Omaha, NE, 68105, USA.

E-mail address: skumbar@unmc.edu (S.G. Kumbar).

<https://doi.org/10.1016/j.bioactmat.2025.03.017>

Received 24 January 2025; Received in revised form 26 February 2025; Accepted 20 March 2025

Available online 26 March 2025

2452-199X/© 2025 The Authors. Publishing services by Elsevier B.V. on behalf of KeAi Communications Co. Ltd. This is an open access article under the CC BY-NC-ND license (<http://creativecommons.org/licenses/by-nc-nd/4.0/>).

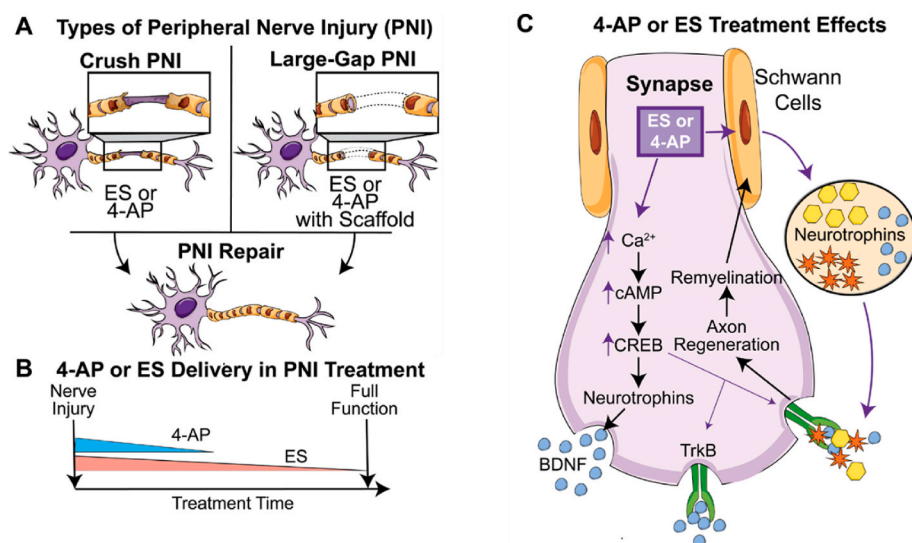
site, typically modeled using nerve "crush" methods [6]. Crush injuries damage Schwann cells and some axons but preserve axonal connectivity, allowing for natural recovery without needing implants [6] (Scheme 1A). This model is often used to study nerve regeneration, both with and without stimulation (Scheme 1A, B). In contrast, large-gap or critical-sized nerve injuries are modeled by removing segments of large nerves, such as the sciatic nerve, and surgically implanting autografts, allografts, or scaffolds with or without stimulation [5] (Scheme 1A). Most knowledge about PNI regeneration, including chemical and electrical stimulation effects, comes from crush models that do not require implants [5] (Scheme 1C). However, large-gap PNI repair is a more complex, long-term process requiring grafts or engineered scaffolds that promote nerve growth and reconnection. Though crush and large-gap injuries likely share similar regenerative mechanisms, little is known about the specific processes involved in large-gap repair. A review of allografts showed that all 16 rat studies found pro-regenerative agent-enriched allografts significantly improved large-gap nerve repair compared to plain allografts [7]. Understanding these mechanisms will aid in designing better scaffolds and allografts to enhance healing for large-gap PNI.

Electrical stimulation (ES) has shown promise as a therapy for the functional rehabilitation of various tissue injuries, including muscle, bone, skin, tendons, ligaments, and nerves by enhancing the cell proliferation, extracellular matrix production, cytokine release, and vascular development [8]. However, the specific mechanisms behind these effects are not fully understood. In peripheral nerve injuries, ES has been shown to accelerate axonal regeneration and functional recovery in both animal models and clinical trials. This acceleration is associated with increased expression of neurotrophic factors, particularly brain-derived neurotrophic factor (BDNF) and its receptor tropomyosin receptor kinase B (TrkB) (Scheme 1C). Some studies also suggest that ES, when applied at low to moderate intensities, can reduce inflammatory and immune responses by altering cytokine release and affecting cell behavior, including survival, proliferation, and death [9]. However, the effects of ES on immune responses to implants have not yet been studied. The potential for ES to enhance tissue regeneration in large-gap PNI remains unclear. Challenges in achieving reliable *in vivo* stimulation and consistent healing outcomes, particularly in nerve crush injuries, still exist [5]. One major issue is that ES signal transduction from skin-surface electrodes to underlying nerves is often unreliable without suitable connecting materials [10]. Recent research highlights

ion-conducting hydrogels as an electrode interface that improves signal delivery to nerves, offering a less painful option for long-term ES application [11]. To unlock the full potential of ES in large-gap PNI, further studies are needed to establish optimal ES parameters and develop advanced technologies for reliable ES delivery to improve regenerative capacity and functional recovery.

Chemical stimulation can support nerve repair, particularly with agents like 4-aminopyridine (4-AP), a potassium-channel blocker. 4-AP has been shown to promote remyelination in multiple sclerosis by prolonging action potentials and increasing neurotransmitter release [6]. Myelin is essential for speeding up action potential conduction along axons [12]. In nerve crush injuries—where axons remain intact, but the myelin sheath is damaged, 4-AP application has been shown to improve remyelination and increase nerve conduction velocity, leading to functional recovery [13] (Scheme 1). In our recent study, rats treated with 4-AP-loaded scaffolds for long-gap nerve repair showed functional and histological outcomes similar to those of autograft controls after 8 weeks [14]. These findings suggest that 4-AP could enhance repair in large-gap PNI. However, further research is necessary to ensure effective long-term delivery and sustained functional improvements.

FDA-approved nerve guidance conduits (NGCs) like Neurotube®, Neurolac®, and NeuraGen® are available for treating smaller nerve defects (8–30 mm) [15]. These NGCs have clinical limitations, including material weakness, lack of bioactivity, harmful degradation byproducts, and suboptimal PNI repair. Issues like poor nutrient and neurotransmitter delivery and inadequate myelin and blood vessel formation emphasize the need for improved treatments [16]. Electrically conducting polymers have been adopted to create electroactive NGCs to deliver ES across the nerve gap for neural recording and stimulation applications. However, using metal electrodes that protrude from the skin and larger power sources for stimulation can complicate implementation and increase the risk of infection [17]. Popular conductive materials typically include non-degradable oxidized ringed polymer structures such as polyaniline, polypyrrole, poly(3,4-ethylenedioxythiophene) (PEDOT), and polymer composites that contain metal or carbon fillers [18–20]. These nondegradable polymers suffer from processing issues, brittleness, hydrophobicity, and, most importantly, short-term redox stability that limits long-term conductivity in physiological conditions [19]. To address these challenges, we have developed ionically conductive (IC) engineered NGCs with structural, mechanical, and biodegradable features ideal for repairing PNI



Schematic 1. PNI types, and how ES and 4-AP delivery affects Schwann cell activity and nerve regeneration. (A) Crush and large-gap PNI models. (B) ES and 4-AP delivery timing, with (C) each treatment sustaining nerve depolarization and increased expression of intracellular Ca^{2+} , neurotrophin BDNF, and TrkA, B, and C receptors. Secreted neurotrophins act on TrkA, B, and C to promote axon regeneration and remyelination. Both treatments enhance Schwann cell activities and motor function recovery in crush PNI.

gaps >4 cm and providing reliable stimulation for a longer time [19]. The IC polymers conduct electricity through the counter flow of ions in a physiological environment, enabling them to maintain tunable and sustained conductivity compared to electronically conducting polymers and polymer composites with metal or carbon fillers [19]. Additionally, IC polymers can be hydrophilic, biodegradable, and bioactive to improve nerve regeneration compared to nondegradable electrically conducting materials [21]. A recent study describes ion-conducting hydrogels as an electrode interface that improves signal transduction to deliver reliable ES to nerves, which may be less painful for long-term application [11]. Sulfonated and sulfated chitosan-based IC polymers support cell attachment, proliferation, maturation, and biocompatibility [22]. In the present work, we introduce phytate ions on the chitosan backbone and create NGCs designed to deliver bioactive molecules and ES to enhance the axon regeneration rate and biocompatibility. A single treatment of 4-Aminopyridine (4-AP) or ES immediately following crush nerve injuries has demonstrated complete functional restoration [13]. However, applying them to large-gap PNI defects poses challenges,

primarily due to the high-water solubility of 4-AP and the requirement of applying ES within the body cavity. Local delivery of 4-AP using scaffolds at the PNI site often leads to dose dumping over a short period [14]. Similarly, delivering ES using electronically conducting polyaniline scaffolds fails because they lack redox stability in the biological environment, necessitating metal electrodes protruding through the skin [19]. As a solution, our approach involves using ionically conductive (IC) chitosan conduits with 4-AP encapsulated within halloysite nanotubes (HNT) to sustain release over an extended period [23]. Our previous study demonstrated that 15 mm sciatic nerve defects treated with 4-AP eluting chitosan scaffolds promoted axon regeneration and functional recovery comparable to autografts after 8-weeks, with thick myelin and the presence of S100 and neurofilament markers [14]. Additionally, these IC conduits facilitate sustained electrical stimulation through the counterflow of ions in a biological environment and promote cell-material interaction under ES [19,24].

The novelty of the current work is creating a scaffold platform with an optimal combination of structural and physicochemical attributes for

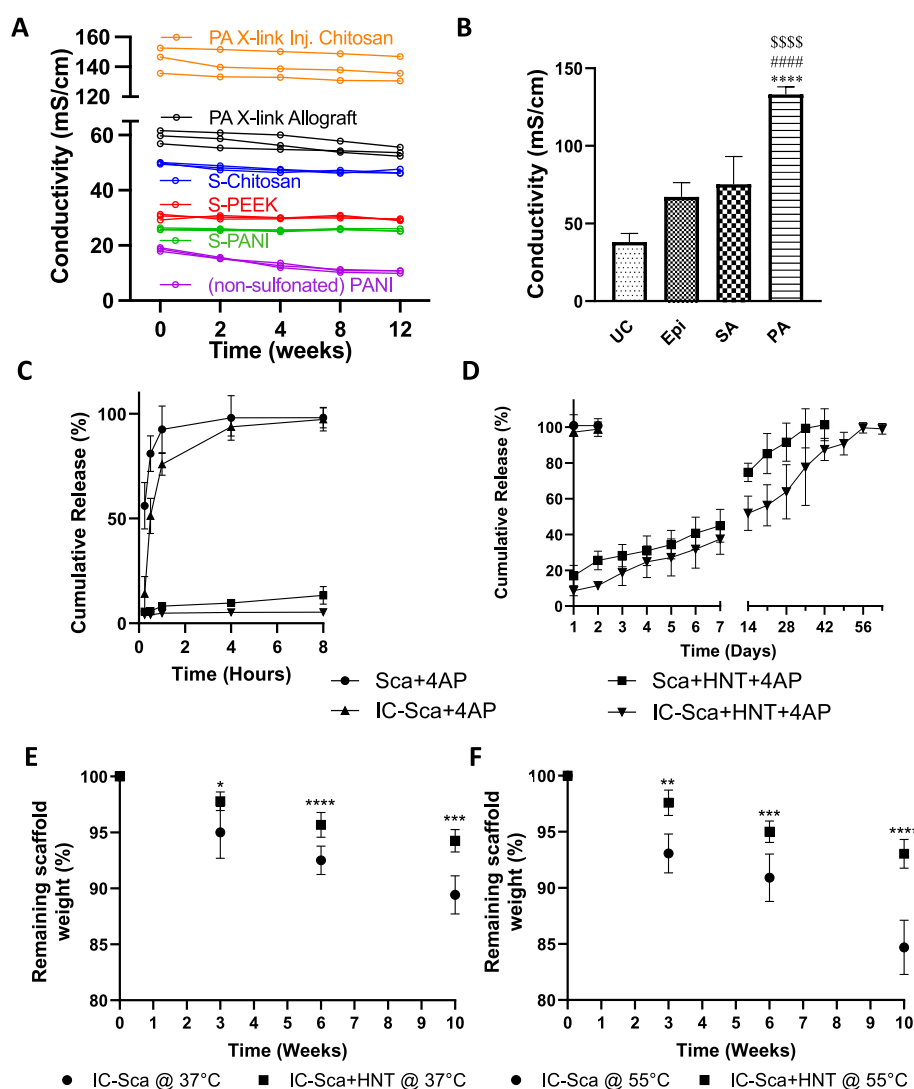


Fig. 1. Phytic acid (PA) cross-linked (X-link) chitosan, allografts, and sulfonated chitosan exhibit superior initial and sustained conductivity. PA X-link chitosan-HNT composites provide the highest ionic conductivity and sustained 4-AP release. (A) Ionic conductivity of sulfonated polyaniline (S-PANI), sulfonated poly(ether-ether-ketone) (S-PEEK), sulfonated chitosan (S-Chitosan), PA cross-linked chitosan, and nerve allografts measured in PBS (pH 7.4) over 12 weeks (N = 3 per group). **(B)** Effect of cross-linking agents on scaffold conductivity (UC = Uncross-linked, Epi-Epichlorohydrin, SA-Sulfuric Acid, PA-Phytic Acid). Significance levels: ****p < 0.0001 vs. UC, ###p < 0.0001 vs. Epi, \$\$\$p < 0.0001 vs. SA. **(C)** Neat and uncross-linked scaffolds release all 4-AP within 8 h, while **(D)** chitosan/HNT and IC composite scaffolds provide sustained 4-AP release for over five weeks. **(E)** Scaffold degradation profiles in PBS (pH 7.4) at 37 °C and **(F)** under accelerated conditions at 55 °C for up to 10 weeks. The sample size was n = 6, and data presented as Mean ± SD (Significance: *p < 0.05, **p < 0.01, ***p < 0.001, ****p < 0.0001 vs. IC-Sca).

the sustained delivery of ES as well as pharmacological agents and growth factors. Our IC polymeric scaffold fabrication method is a scalable, single-step process allowing the incorporation of drugs and growth factors [14]. Sustained delivery of a freely water-soluble, small drug molecule (such as our model, 4-AP) over weeks or months using a biodegradable scaffold system is an unmet drug delivery challenge. This model drug was chosen to establish IC scaffold benefits in large-gap PNI, as it has been used in crush injuries [6]. Incorporating 4-AP in the lumen of HNTs enables a reliable, programmable release profile. Likewise, biocompatible and tissue-pliant conducting polymers that will allow reliable ES throughout the treatment period and complete biodegradation by the treatment end remain unaddressed challenges. Also, the combined effects of 4-AP and ES *in vitro* or on critical-sized nerve defects *in vivo* have not been tested. Here, for the first time, we report using phytate ion-bearing chitosan IC formulation as electrodes to mediate transcutaneous ES *in vivo*, as shown in Fig. 2.

Our central hypothesis is that the chemical and electrical cues from

IC bioengineered NGCs will improve interactions between Schwann cells and the material, resulting in altered neurotrophin secretion and immune responses, as shown in Scheme 1. This, in turn, will promote axon regeneration and enhance functional recovery. Phytate ion-bearing chitosan NGCs containing 4-AP were fabricated and characterized for their physicochemical properties, including surface morphology, *in vitro* drug release, degradation, and changes in mechanical strength during degradation [24]. Additionally, these NGCs were evaluated for Schwann cell-material interactions *in vitro* under treatments of 4-AP, ES, and 4-AP/ES to assess cell attachment, proliferation, and neurotrophic factor secretion. The scaffolds that showed the greatest phenotype development by Schwann cells, alone or in combination with 4-AP/ES treatments, were further used to study large-gap sciatic nerve defects in rats, specifically 2 cm and 4 cm, to mimic clinically relevant defect sizes. Nerve healing outcomes were assessed through histology, myelination, myelination thickness, and gene analysis to evaluate the expression of neurotrophic factors and their receptors. Electrophysiological

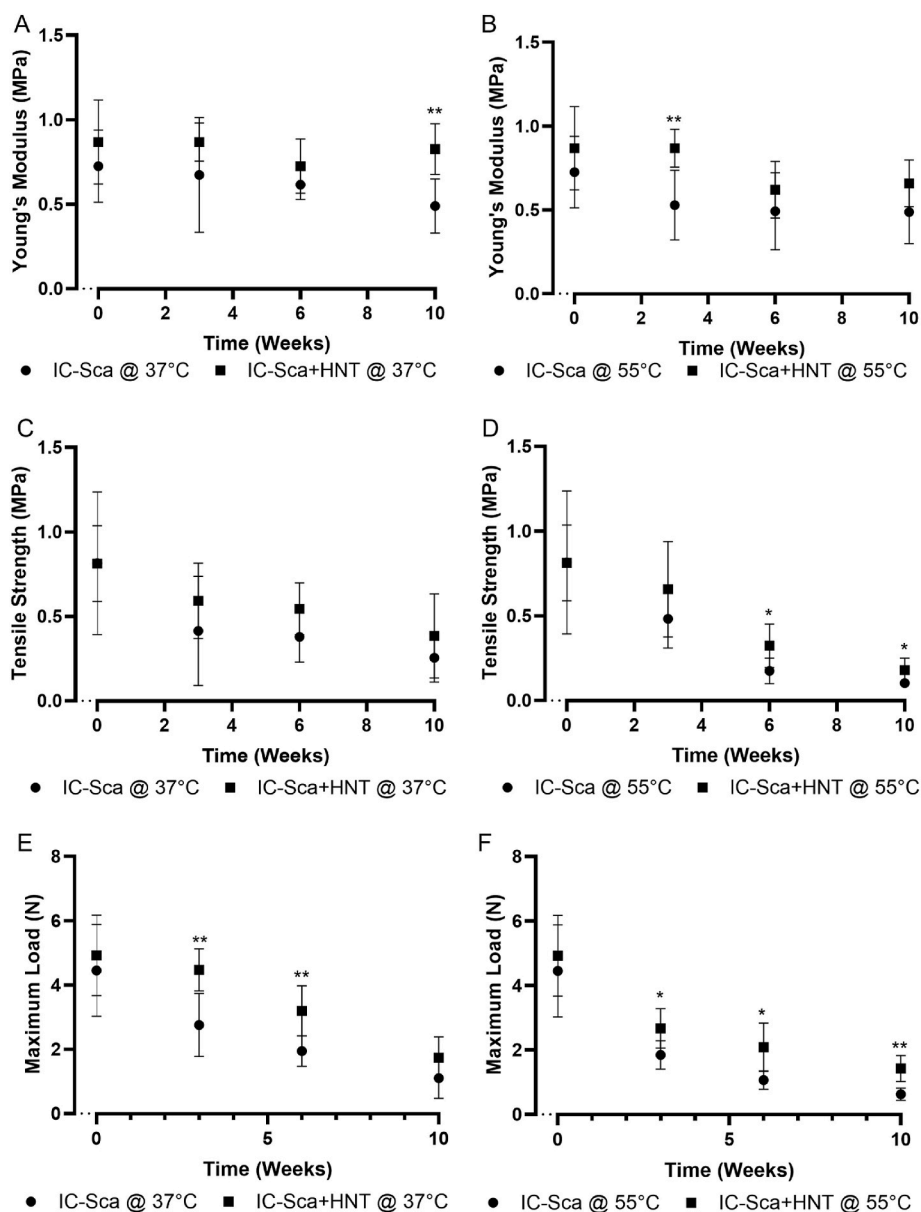


Fig. 2. Composite scaffolds demonstrated superior tensile properties and a slower degradation rate than neat IC scaffolds at 37°C and 55°C. The tensile properties of scaffolds at 37°C and 55°C were assessed as a function of degradation time, including (A & B) Young's modulus, (C & D) UTS, and (E & F) maximum load at the break. However, the observed decrease in ultimate tensile strength (UTS) and load at break over time indicates a loss of mechanical integrity as degradation progresses. Statistical significance is indicated as *p < 0.05, **p < 0.01 compared to IC scaffolds (IC-Sca).

measurements such as compound muscle action potential (cMAP), nerve conduction velocity, and gastrocnemius muscle weight recovery assessed regenerated nerve functional recovery. The nerve healing outcomes were compared with autografts and individual treatments to elucidate the benefits of combined therapy of 4-AP/ES.

2. Results

2.1. Physical characterization of NGCs

2.1.1. Conductivity measurements

We synthesized a variety of sulfonated polymers using natural and synthetic backbones, including sulfonated chitosan (S-Chitosan), sulfonated polyaniline (S-PANI), and sulfonated poly(ether ether ketone) (S-PEEK). Chitosan (2 % w/w) was dissolved in 2 % acetic acid and reacted with an equimolar amount of 1,3-propane sultone for 6 h at 60 °C. The precipitated S-Chitosan was filtered, washed with acetone and methanol, and vacuum-dried at 50 °C. For S-PANI, aniline (5 mL) and propane sultone (1.35 g) were mixed in acetone for 6 h at room temperature. The resulting sulfonated aniline was filtered, washed with acetone, and dried. It was then polymerized with potassium persulfate (1:1) inequiproportionate solution of ethanol and water, followed by 24-h dialysis and lyophilization to obtain S-PANI. S-PEEK was prepared by dissolving 5 g of PEEK in 100 mL of concentrated sulfuric acid (98 %), stirring to a homogeneous solution for 10 min, then heating at 50 °C for 2 h. The cooled solution was precipitated in ice-cold water, thoroughly washed, and dried [25,26]. The characteristic FTIR bands in the 1080–1190 cm^{-1} range confirmed the modification of polymer backbones with sulfonic acid ionic groups. The modified polymers were cast into 3–4 mm thick membranes using solution casting, with water (S-Chitosan), dimethylacetamide (S-PEEK), and dimethylformamide (PANI and S-PANI) as solvents. As previously reported, all polymers' ion exchange capacity (IEC) was determined using titration. The IEC values followed the order: PA X-link chitosan > PA X-link Allograft > S-Chitosan > S-PEEK > S-PANI > PNI. The sulfonated polymers S-Chitosan, S-PEEK, and S-PANI exhibited IEC values of 1.65, 1.2, and 0.85 m equiv./g, respectively, while PNI showed a lower IEC of 0.65 m equiv./g. Notably, chitosan and nerve allograft cross-linked with phytic acid (PA X-link) demonstrated significantly higher IECs than the sulfonated polymers. For instance, injectable PA X-link Chitosan and its membrane form showed an IEC of 4.62 m equiv./g, and PA X-link Allograft displayed 1.98 m equiv./g. The conductivity of the IC polymers followed the same trend: PA X-link injectable Chitosan > PA X-link Allograft > S-Chitosan > S-PEEK > S-PANI > PANI (Fig. 1A). This order correlates with the IEC, reflecting the increasing presence of sulfonic acid or phytate ion functionalities in the polymer matrix.

All the sulfonated and phytate ion-modified IC polymers generally maintained steady ionic conductivity over 12 weeks, while the conductivity of electrically conductive PANI decreased significantly (Fig. 1A). PA cross-linked chitosan, in injectable, scaffold, and electrode forms, maintained an average conductivity of 140 ± 5 mS/cm throughout the 12 weeks. Similarly, S-PANI showed an average conductivity of 25 ± 3 mS/cm. In contrast, pristine PNI, which had an initial conductivity of 16 ± 2 mS/cm, declined to 11 ± 2 mS/cm over the same period. Phytate ion-modified decellularized rat sciatic nerve allografts, cross-linked with PA, maintained a conductivity of 57 ± 3 mS/cm, significantly higher than any of the sulfonated polymers tested. We investigated the effect of various cross-linkers on chitosan scaffolds, including epichlorohydrin (Epi), sulfuric acid (SA), and PA (Fig. 1B). PA cross-linked scaffolds exhibited the highest conductivity, showing a ~ 3.5 -fold increase (133.2 ± 4.2 mS/cm) compared to uncross-linked chitosan scaffolds (38.11 ± 4.74 mS/cm). SA cross-linked scaffolds demonstrated a ~ 2 -fold increase (75.34 ± 15.49 mS/cm), while Epi cross-linked scaffolds showed a ~ 1.7 -fold increase (67.18 ± 7.93 mS/cm). These conductivity values surpass those reported in previous studies on electrically conductive polymers used in nerve guidance

conduits [27–29]. Due to their higher ion exchange capacity (IEC), controlled water uptake, and superior conductivity, the phytate ion-modified chitosan scaffolds were further characterized for nerve regeneration applications [26].

2.1.2. Drug encapsulation & release profiles

The encapsulation efficiency almost doubled with addition of HNT as the composite displayed an efficiency of 9.8 ± 2.5 % in comparison to scaffold without HNT having efficiency of 4.9 ± 2.5 %. Both the neat (Sca+4AP) and cross-linked (IC-Sca+4AP) scaffolds released over 75 % of the drug within the first 2 h and 100 % within two days due to the rapid diffusion of the water-soluble 4-AP (Fig. 1C). In contrast, the composite scaffolds, both uncross-linked (Sca+HNT) and cross-linked (IC-Sca+HNT), provided a sustained release of 4-AP over 7 weeks, as the drug was encapsulated within the HNT lumen (Fig. 1D). The 4-AP-filled HNTs were sealed with chitosan at both ends in the composite scaffolds, slowing diffusion and enabling the sustained release [23]. All scaffold formulations, whether cross-linked or not, maintained structural stability over 8 weeks, consistent with previously reported Epi cross-linked chitosan scaffolds [23].

2.1.3. Accelerated degradation

Fig. 1E and F shows the degradation and erosion profiles of neat (IC-Sca) and composite (IC-Sca+HNT) scaffolds over 10 weeks at 37 °C and 55 °C, respectively. Since chitosan undergoes enzymatic degradation in the body, this characterization is crucial to understanding scaffold erosion and conductivity *in vitro*. Studying degradation at 55 °C helps accelerate the process for a shorter analysis period [30]. The composite scaffolds (IC-Sca+HNT) exhibited a significantly reduced erosion rate compared to neat scaffolds (IC-Sca) at both temperatures. After ten weeks at body temperature, the weight loss for neat and composite scaffolds was around 90 % and 95 %, respectively. At 55 °C, the weight loss was approximately 95 % for neat scaffolds and 85 % for composite scaffolds. The composite scaffolds maintained a steady and insignificant weight loss at both temperatures, while neat chitosan showed significant erosion. This constant erosion rate of the composite scaffold is ideal for providing structural support at the defect site, enabling sustained 4-AP release and consistent stimulation.

2.2. Tensile properties

Fig. 2A–F illustrates the changes in tensile properties for neat (IC-Sca) and composite (IC-Sca+HNT) scaffolds after 10 weeks of degradation at 37 °C and 55 °C. This analysis is crucial for evaluating the structural integrity required to support critical-sized nerve defects (>4 cm). No significant differences in Young's modulus were observed for either scaffold at both temperatures (Fig. 2A and B), suggesting that the scaffold stiffness remained unaffected by degradation. However, notable reductions in tensile strength were observed at the 6 and 10-week time points at 55 °C, indicating degradation and structural alterations (Fig. 2C and D). The maximum load for failure also exhibited significant differences between the two temperatures for both scaffolds beyond 3 weeks, pointing to degradation (Fig. 2E and F). Overall, the tensile properties followed similar degradation trends for both scaffolds and temperatures.

2.3. In vivo subcutaneous implantation study

We implanted scaffolds subcutaneously in rats and applied ES following our established protocol to evaluate whether ES, 4-AP, or the combination of 4-AP and ES induces an immune response compared to IC scaffolds alone. Blood samples were collected from tail veins at multiple time points over 14 days to measure IL-6 and IL-10 cytokines using ELISA (Fig. 3A). The levels of IL-6 and IL-10 fluctuated. Still, the IL-6/IL-10 ratio—a marker for immune response—initially dropped and stabilized, indicating no significant immune reaction to the implanted

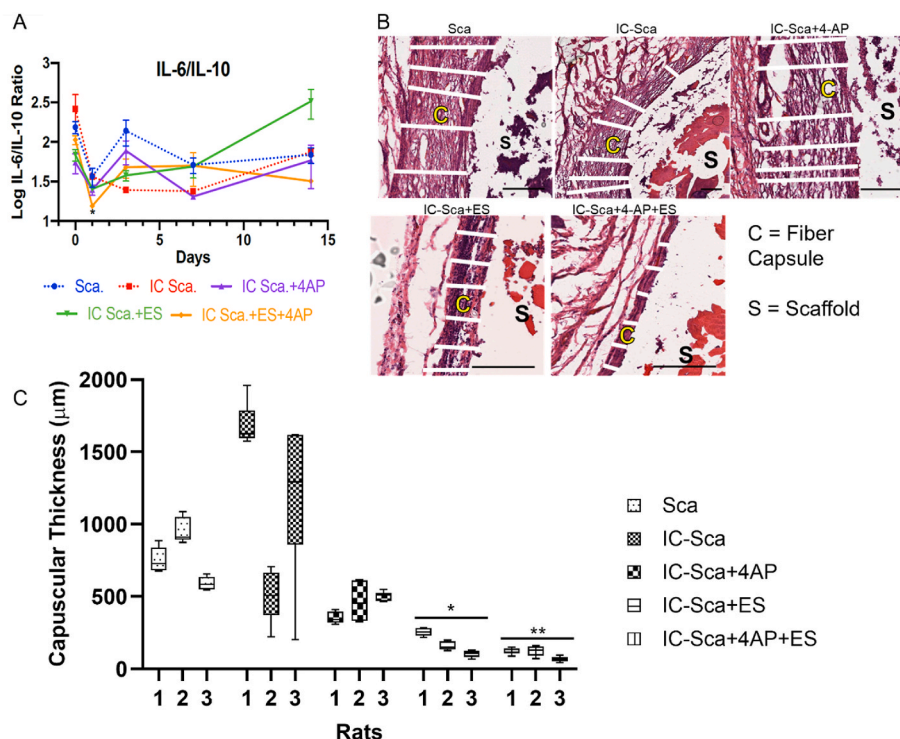


Fig. 3. IC scaffolds with the combined 4-AP+ES treatment showed improved foreign body response compared to IC scaffolds alone in a 14-day subcutaneous rat implantation study. (A) Serum levels of IL-6 and IL-10 were measured via ELISA from blood samples collected over 14 days (mean \pm SEM). (B) Representative H&E images highlight the fibrous capsule formation around the implant (marked by white lines, scale bar = 600 μ m). (C) Fibrous capsule thickness was analyzed by group and individual rats, with data presented as box and whisker plots (median, interquartile range, and min/max). * $p < 0.05$ or ** $p < 0.01$ compared to IC scaffold group, analyzed by two-way ANOVA and Tukey's multiple comparison test.

scaffolds during the 14 days (Fig. 3A). We also measured the thickness of fibrous capsules around the implants, a sign of immune response, using H&E-stained sections. Although IC-Sca results varied between individual rats, the average fibrous capsule thickness was consistently and significantly reduced when ES, 4-AP, or ES+4-AP were applied (Fig. 3B and C). A thinner fibrous capsule suggests a reduced foreign body response and improved host-tissue integration [31]. Further analysis of infiltrating cells could help explain the cytokine fluctuations. Our findings suggest that IC chitosan scaffolds, combined with ES and/or 4-AP, do not trigger a significant immune response but enhance tissue integration and biocompatibility.

2.4. In vitro characterization of NGCs

2.4.1. Cell viability & proliferation

4-AP and ES effects on Schwann cell viability and proliferation on TCPS and IC composite scaffolds were assessed over 21 days. Schwann cells maintained viability and a well-spread morphology, indicating compatibility with chronic ES, either alone or combined with 4-AP (Fig. 4A, Suppl. Fig. 1). Fewer dead cells were observed in the IC+4-AP+ES group compared to other treatments at 14 and 21 days. MTS assay showed steady Schwann cell growth over 7 days, with no significant impact on proliferation from ES or 4-AP (Fig. 4B). SEM images confirmed Schwann cell attachment and spread by day 3 (Fig. 4C), and cells formed clusters, retaining their native phenotype at later time points. These results support the cytocompatibility of the IC scaffolds and treatments.

2.4.2. Immunocytochemical analysis

The neurotrophic markers BDNF, NGF, and MPZ expression by Schwann cells under different treatments were assessed on day 14. These proteins are crucial for Schwann cell survival, proliferation, and differentiation, forming a functional myelin sheath in regenerating axons.

Expression was significantly higher in the combined C+4-AP+ES group compared to ES or 4-AP alone (Fig. 5A). Notably, a ~ 1.7 -fold increase in BDNF and MPZ and a ~ 2 -fold increase in NGF were observed in the combined treatment group, based on fluorescent intensity from ICC images (Fig. 5B). Similar expression profiles were seen with individual 4-AP and ES treatments.

2.4.3. Gene expression studies

NGF, BDNF, glial cell line-derived neurotrophic factor (GDNF), neurotrophin-3 (NT-3), NT-4, and S100 calcium-binding protein b (S100b) are essential for axon regeneration, promoting neuronal survival, differentiation, and growth. NGF supports peripheral neuron repair, BDNF aids synaptic plasticity, and GDNF helps motor neuron survival. NT-3 and NT-4 enhance sensory neuron development and axonal growth, while S100B regulates cell growth and myelination [32]. Schwann cells expressed these neurotrophic genes on days 7 and 14, with NGF as a positive control and basal media (BM) as a negative control. Combined ES and 4-AP treatment showed the highest gene expression, with significant increases on day 7 (BDNF: 6-fold, NGF: 2-fold, GDNF: 3-fold, NT-3: 6-fold, NT-4: 6.5-fold, S100B: 4-fold) (Suppl. Fig. 2) and day 14 (BDNF: 3.5-fold, NGF: 4-fold, GDNF: 6-fold, NT-3: 8-fold, NT-4: 10-fold, S100B: 10-fold) (Fig. 6) compared to BM. NGF treatment was higher than individual 4-AP or ES but similar to their combined treatment.

2.4.4. Proteomics analysis

Quantitative proteomic analysis was performed on Schwann cell culture media collected on day 14 under 4-AP, ES, and 4-AP+ES treatments, with TCPS (negative) and NGF (positive) as controls. Several proteins were identified (data not shown), but key neurotrophic proteins, including neural cell adhesion molecule 1 (NCAM1), neuophilin 2 (NRP2), carboxypeptidase E (CPE), fibronectin (FN1), insulin-like growth factor (IGF), and transforming growth factor- β (TGF- β), were

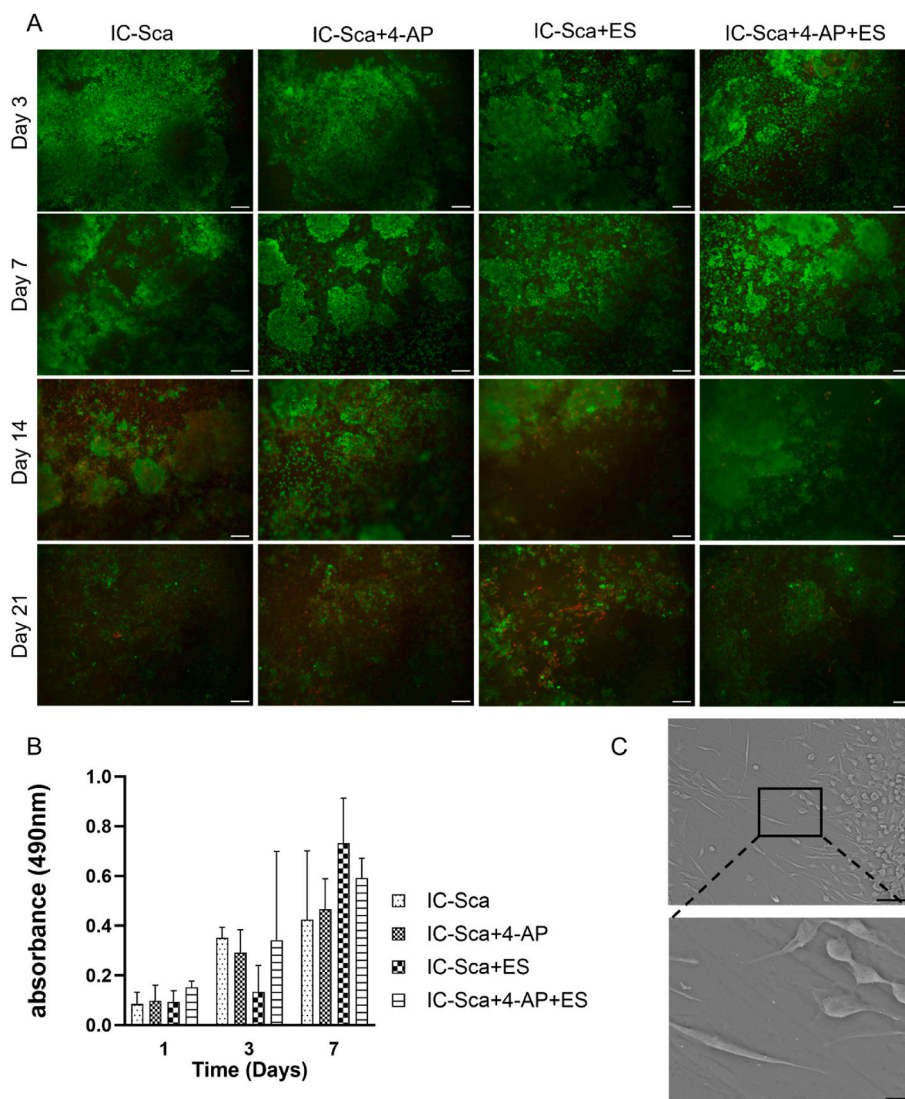


Fig. 4. Composite IC scaffolds effectively supported Schwann cell viability and proliferation during chronic 4-AP and ES treatments. Schwann cells were seeded on the IC scaffolds and subjected to 4-AP (30 $\mu\text{g}/\text{mL}$) and/or ES (1 V, 20 Hz for 20 min). (A) Cell viability was assessed over 21 days, with live cells appearing green and dead cells red at 20 \times magnification ($n = 3$). Scale bar = 100 μm . (B) Cell metabolic activity was quantified using an MTS assay over 7 days ($n = 5$), and results are presented as Mean \pm SD. (C) SEM images ($n = 3$) display Schwann cells' elongated morphology at 500 \times (top) and 2000 \times (bottom), with scale bars of 50 μm and 10 μm , respectively.

analyzed for their expression (Fig. 7). NCAM1 aids neural migration, axon branching, and synaptogenesis, particularly during synaptic plasticity [33]. CPE processes neuropeptides and transports BDNF via synaptic junctions [34]. NRP2 functions as a receptor for semaphorins, aiding axon guidance and interacting with VEGF receptors. FN1, a cytoskeletal glycoprotein, promotes Schwann cell growth, motility, and differentiation [35], especially at lesion sites. IGF stimulates myelination and attracts axon growth cones, while TGF- β regulates glial and neuronal cell transformation at injury sites [36]. As expected, these proteins were significantly upregulated in the treatment groups (4-AP, ES, and 4-AP+ES) compared to TCPS controls. This suggests various treatments and the scaffold system supports critical neurotrophic factors essential for Schwann cell growth and myelination.

2.4.5. Neurite outgrowth analysis

The conditioned media from Schwann cell cultures under various treatments, collected on day 14, was assessed for its ability to promote neurite outgrowth in F11 and PC-12 cells through image analysis (Fig. 8A and Suppl. Fig. 3). NGF, crucial for neurite outgrowth and differentiation, also promotes microtubule assembly in these cells. The

media from the combined 4-AP and ES treatment resulted in significantly higher branching and longer neurites compared to individual treatments (4-AP, ES) and the positive control NGF (Fig. 8A and Suppl. Fig. 3). The average neurite length of PC12 cells in the combined treatment was 2.5 times greater than in the NGF control (100 ng/mL in basal media) (Fig. 8B). Neurite extension in other treatments was notably lower than in the combined treatment, and basal media alone did not support neurite extension (Fig. 8B). This indicates that Schwann cell-secreted neurotrophic factors are bioactive and effectively promote neurite extension in neuronal progenitors.

2.4.6. Western blot analysis

The synergistic effects of the combined 4-AP and ES treatments were further validated by the quantification of BDNF, NGF, and S100b protein expression in Schwann cells on day 14 (Fig. 9A). These proteins are crucial for axon regeneration, remyelination, and motor function recovery [37,38]. The combined 4-AP+ES treatment significantly increased the expression of these proteins (Fig. 9B) compared to 4-AP or ES alone, supporting the hypothesis outlined in Scheme 1.

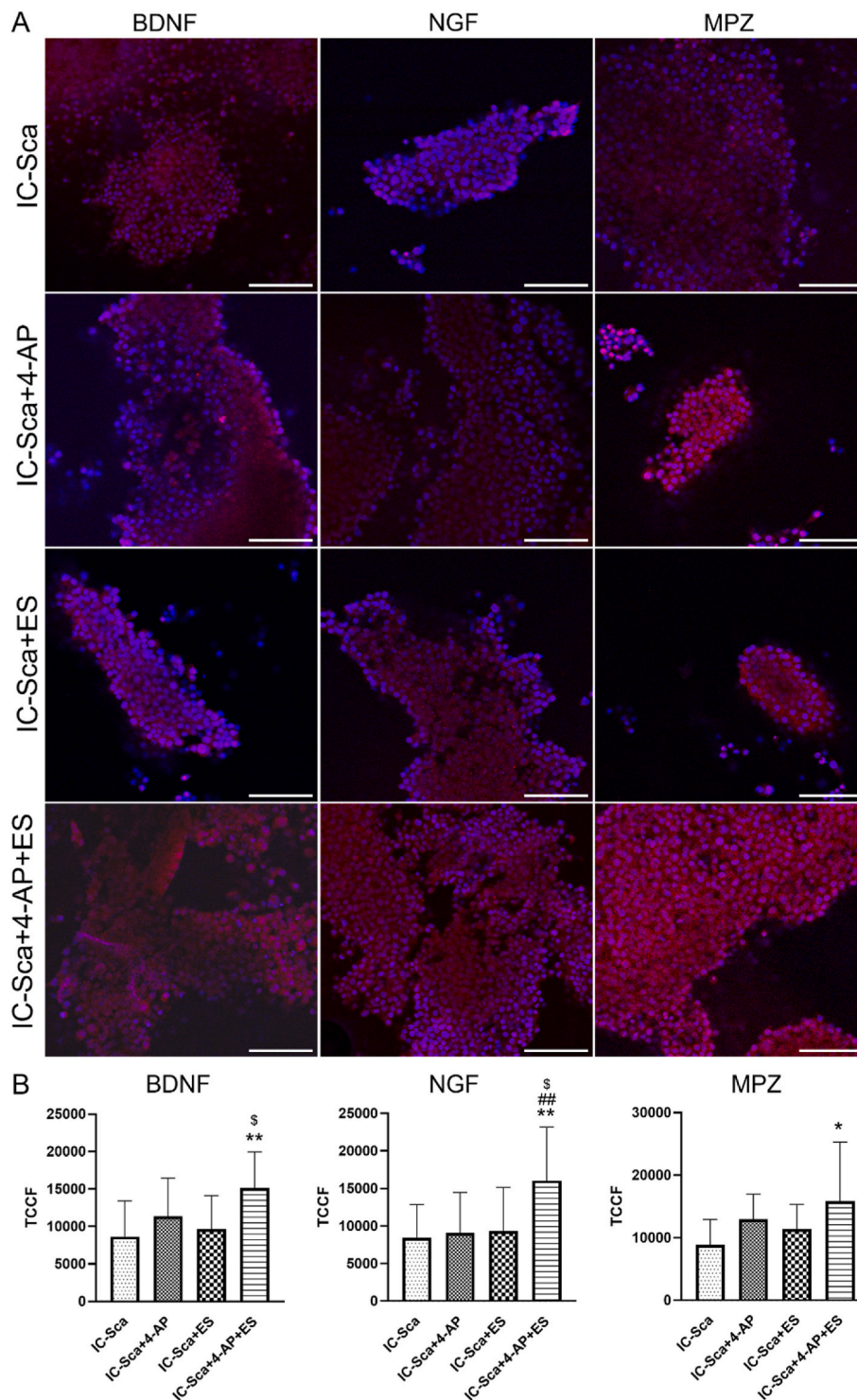


Fig. 5. Schwann cells exhibited significantly higher expression of neurotrophic factors BDNF, NGF, and MPZ under the combined 4-AP+ES treatment than individual 4-AP or ES treatments. (A) Representative immunofluorescent images at day 14 show BDNF, NGF, and myelin protein zero (MPZ) expression on scaffolds (20 \times magnification), where blue fluorescence indicates cell nuclei stained with DAPI, and red fluorescence highlights the specific protein expression. Scale bar = 100 μ m. (B) Quantification of immunofluorescent stains using total corrected cellular fluorescence (TCCF) (n = 15). Data are Mean \pm SD. *p < 0.05, **p < 0.01 vs IC-Sca. ##p < 0.01 vs IC-Sca+4-AP. §p < 0.05 vs IC-Sca+ES.

2.4.7. ELISA analysis

NGF is a key neurotrophic factor in axon regeneration, but our proteomics analysis could not detect it due to interference from FBS-related proteins used during *in vitro* culture. To address this, NGF levels were measured using an ELISA kit on days 7 and 14 (Fig. 10). The combined 4-AP+ES treatment significantly increased NGF secretion on

both days compared to 4-AP or ES alone. Specifically, NGF levels were 1.7-fold higher on day 7 (Figs. 10A) and 6.7-fold higher on day 14 (Fig. 10B) compared to the untreated IC scaffold group. However, as expected, the positive NGF control surpassed all other treatments in NGF expression.

These *in vitro* studies confirm the synergy between 4-AP and ES in

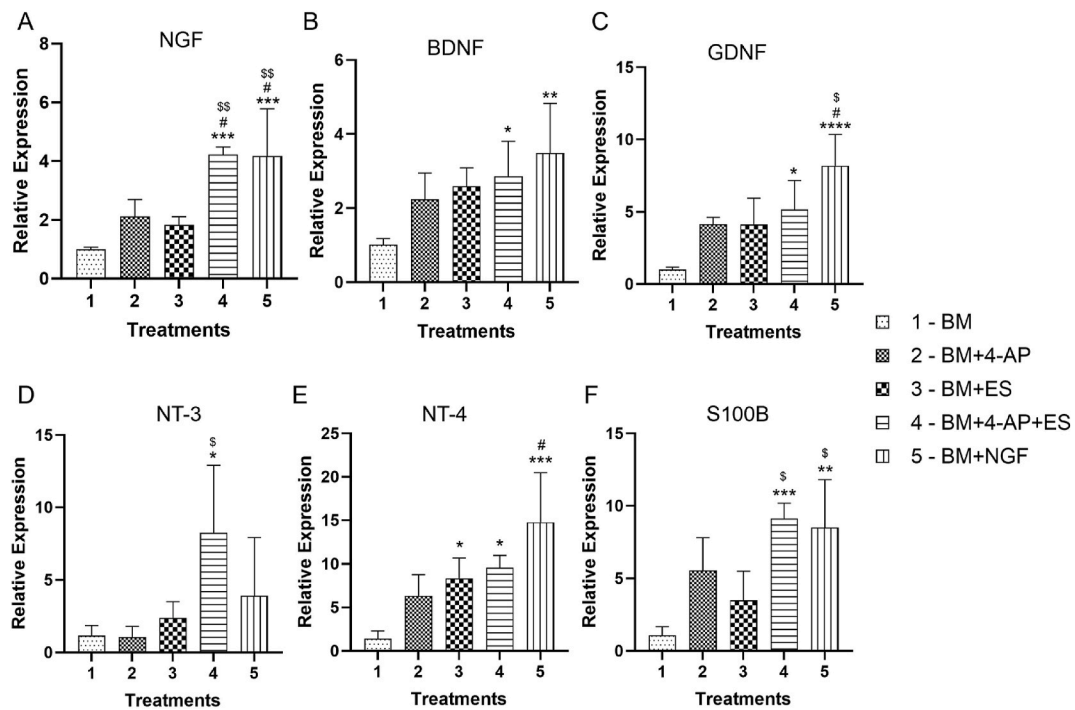


Fig. 6. Schwann cells exhibited significantly higher expression of neurogenic genes under the combined 4-AP+ES treatment than individual 4-AP or ES treatments. Cellular constructs harvested on day 14 were analyzed, with BM as the negative control and 100 ng/mL NGF as the positive control. Key neurogenic genes involved in nerve regeneration were quantified, including (A) Nerve growth factor (NGF), (B) Brain-derived neurotrophic factor (BDNF), (C) Glial cell line-derived neurotrophic factor (GDNF), (D) Neurotrophin-3 (NT-3), (E) Neurotrophin-4 (NT-4), and (F) S100 calcium-binding protein β (S100 β). A sample size $n = 5$ was used for these assays, and the data is presented as Mean \pm SD. * $p < 0.05$, ** $p < 0.01$, *** $p < 0.001$, and **** $p < 0.0001$ vs basal media. # $p < 0.05$ vs IC-Sca+4-AP. \$ $p < 0.05$, \$\$ $p < 0.01$ vs IC-Sca+ES.

promoting neurotrophic factor expression by Schwann cells, enhancing their bioactivity to facilitate neurite extension. Based on these results, the combined treatment (IC-Sca+4-AP+ES) promotes neurite growth through Schwann cell-secreted neurotrophic factors. The chosen *in vitro* parameters provide a solid foundation for further *in vivo* studies on peripheral nerve regeneration.

2.5. In vivo characterization of NGCs

2.5.1. Electrophysiological assessments

Electrophysiological measurements assessed the functional recovery of regenerated nerves 12 weeks post-surgery. Compound muscle action potentials (CMAPs) were recorded by stimulating the sutured nerve ends at the surgical site and monitoring the gastrocnemius muscle's response. Autograft implantation was a 2 cm long transected nerve in the procedure and sutured in a reserved manner for both 2 cm and 4 cm long scaffold implantation. As shown in Fig. 11A–D, the amplitude of the action potentials was 2-fold higher in all treatment groups and autografts compared to the scaffold alone for the 2 cm nerve defect (Fig. 11A and B). Interestingly, the CMAP amplitudes for the 4 cm scaffold, used in a loop fashion, were larger than those for the 2 cm defect (Fig. 11C and D), indicating successful innervation of the gastrocnemius muscles across all treatment groups and autografts. The 4 cm scaffolds, specifically in the ES and ES+4AP groups, displayed average CMAP values comparable to the gold-standard autografts. However, a second waveform observed in the 4 cm scaffold represents another action potential with a smaller amplitude and longer duration (Fig. 11C), suggesting an additional depolarization volley sent back through the scaffold [39]. Though failing to generate a complete second action potential, this second waveform indicates improved electrical activity and neural response.

2.5.2. Gastrocnemius muscle analysis

The gastrocnemius muscles from the repaired and contralateral limbs were harvested to calculate the relative wet muscle weight in the groups with 4 cm scaffolds. Sciatic nerve transection typically causes gastrocnemius muscle atrophy and weight reduction, while successful reinnervation leads to muscle weight recovery. Treatments involving ES (0.35 ± 0.10) and the 4-AP+ES combination (0.47 ± 0.13) resulted in significantly higher wet-weight ratios compared to the scaffold-alone (0.28 ± 0.07) and 4-AP-only (0.28 ± 0.06) groups (Fig. 11E). This suggests that ES more effectively promotes muscle reinnervation than 4-AP alone. Moreover, the combined 4-AP+ES treatment restored the gastrocnemius muscle weight ratio to levels comparable to the autograft group, confirming successful muscle regrowth in the animals implanted with IC-Sca+4-AP+ES scaffolds.

2.5.3. Myelin sheath analysis

All treatments using 2 cm and 4 cm scaffolds led to nerve regeneration over 12 weeks, with varying levels of myelination. Transmission electron microscopy (TEM) images captured from the middle cross-sections of the regenerated nerves show thick black circles representing myelinated A-fiber axons. At the same time, the surrounding lighter gray areas indicate unmyelinated C-fiber axons (Fig. 12A & B). The G-ratio, calculated as the inner axon diameter to the outer diameter, reflects myelin thickness, with lower values indicating thicker myelin. All treatment groups demonstrated an increase in the number of myelinated neurons, with the combined 4-AP+ES treatment and autografts showing the thickest myelin compared to individual treatments (Fig. 12C & D).

2.5.4. Histological analysis

Histological assessments were performed on longitudinal sections of regenerated axons from 2 cm to 4 cm scaffolds and autografts to visualize myelin distribution using Luxol fast blue staining. This dye binds to phospholipids, staining the myelin blue (Fig. 13A–i & 13B–i). All

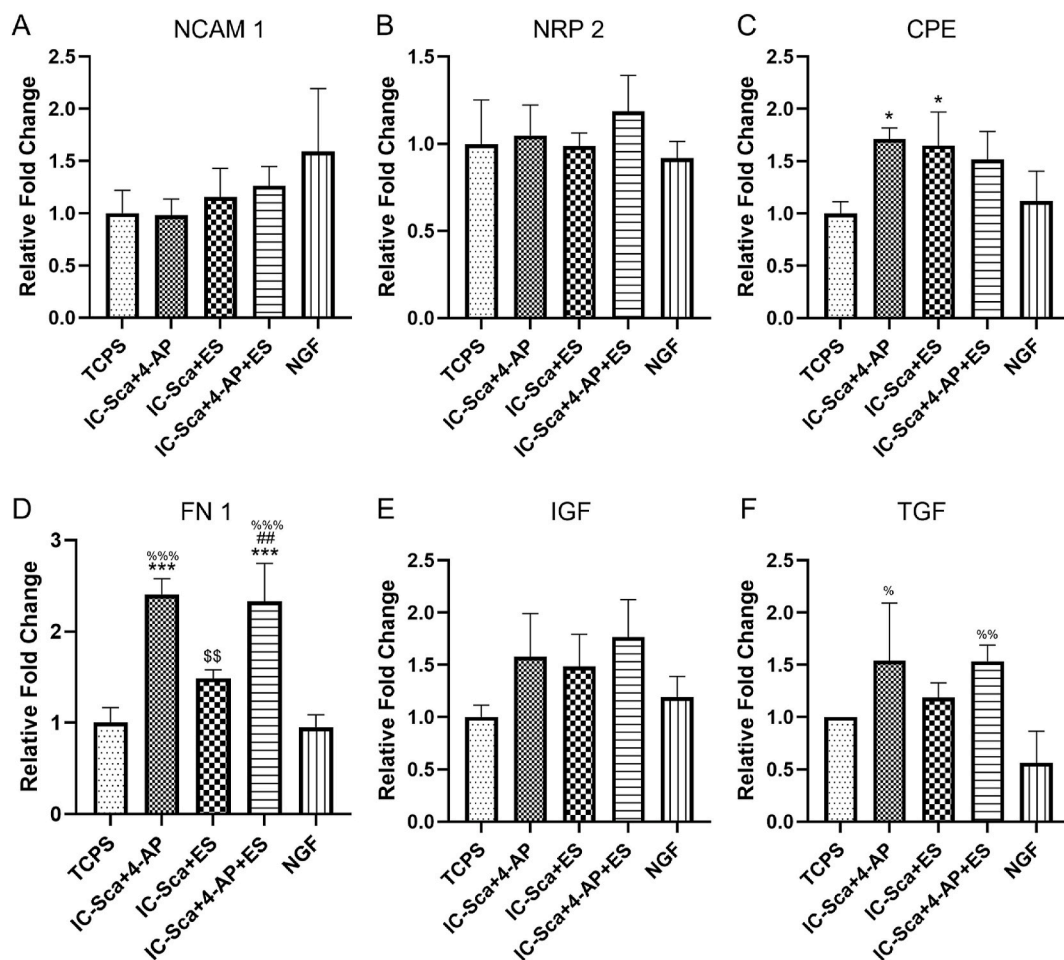


Fig. 7. Schwann cells expressed significantly higher levels of neurotrophic proteins under the combined 4-AP+ES treatment than individual 4-AP or ES treatments. Schwann cell-conditioned media, collected on day 14 from all treatments (BM as negative control and 100 ng/mL NGF as positive control), were subjected to proteomics analysis. Key proteins involved in nerve regeneration were quantified, including: (A) neural cell adhesion molecule 1 (NCAM1), (B) neuropilin 2 (NRP2), (C) carboxypeptidase E (CPE), (D) fibronectin (FN1), (E) insulin-like growth factor (IGF), and (F) transforming growth factor- β (TGF). A sample size $n = 5$ was used, and the data is presented as Mean \pm SD. * $p < 0.05$, ** $p < 0.01$, *** $p < 0.001$, and **** $p < 0.0001$ vs TCPS. # $p < 0.05$ vs IC-Sca+4-AP. \$ $p < 0.05$, \$\$ $p < 0.01$ vs IC-Sca+ES. % $p < 0.05$, %% $p < 0.01$, %%% $p < 0.001$ vs NGF.

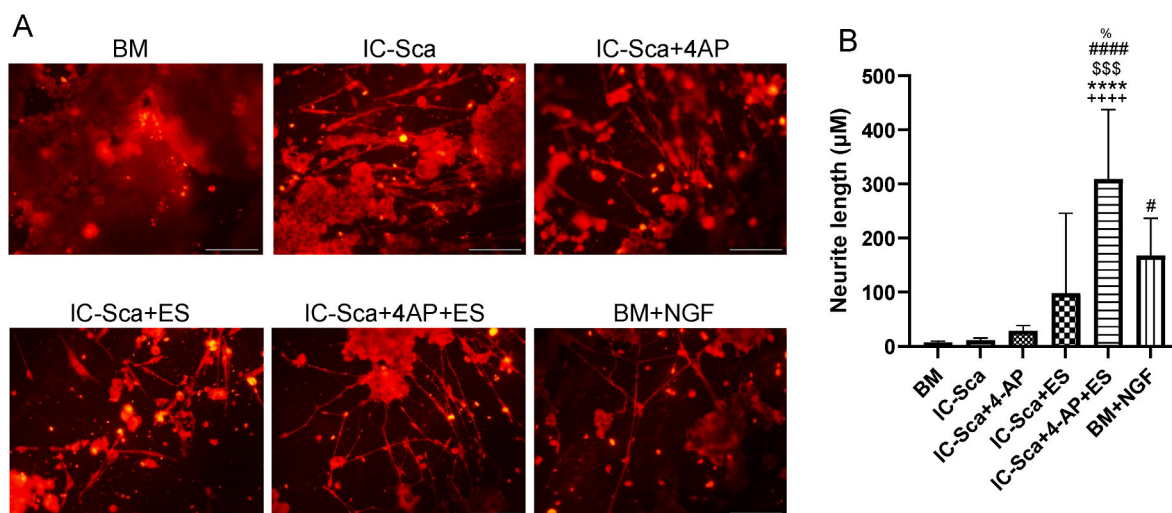


Fig. 8. Schwann cell-conditioned media from the combined 4-AP+ES treatment significantly enhanced PC12 neurite outgrowth compared to individual 4-AP and ES treatments. Schwann cell culture media from all treatments, collected on day 7, were added to PC12 basal media (BM) to support neurite extension, with BM (negative control) and 100 ng/mL NGF (positive control). (A) Representative images of neurite outgrowth stained with Invitrogen™ Neurite Outgrowth Staining Kit at 10 \times magnification. (B) Quantification of average neurite length per cell ($n = 13$). **** $p < 0.0001$ vs IC-Sca. # $p < 0.05$, #### $p < 0.0001$ vs IC-Sca+4-AP. ++++ $p < 0.0001$ vs BM. \$\$\$ $p < 0.001$ vs IC-Sca+ES. % $p < 0.05$ vs BM + NGF.

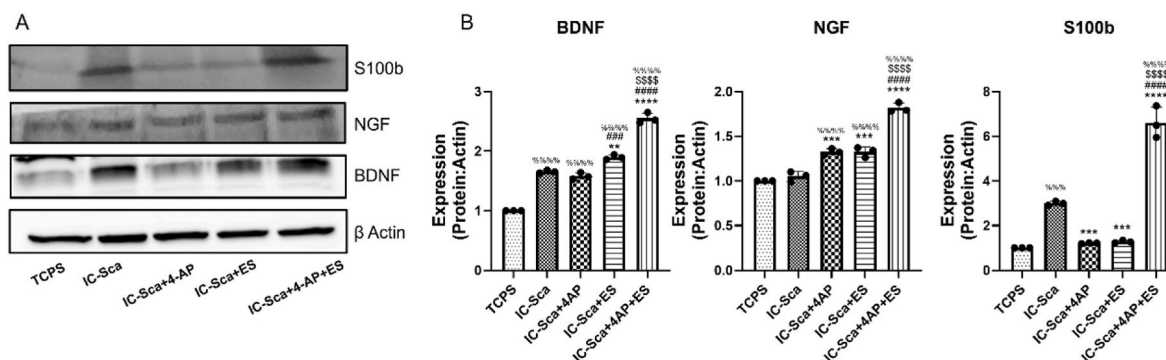


Fig. 9. Schwann cells express significantly higher amounts of BDNF, NGF, and S100 β with combined 4-AP+ES treatment than individual 4-AP or ES treatments at days 7 and 14. (A) Representative western blots of S100, NGF, and BDNF proteins for 14-day samples. (TCPS; control $n = 3$ experiments of 6 pooled samples each). (B) Normalized western blot data is expressed as protein: actin ratio (ng/mL). Data: Mean \pm SEM. One-way ANOVA with Tukey's multiple comparisons tests; %%% $p < 0.0001$ vs. TCPS. *** $p < 0.001$, and **** $p < 0.0001$ vs IC-Sca. #### $p < 0.001$, and ##### $p < 0.0001$ vs IC-Sca+4-AP. \$\$\$ $p < 0.0001$ vs IC-Sca+ES.

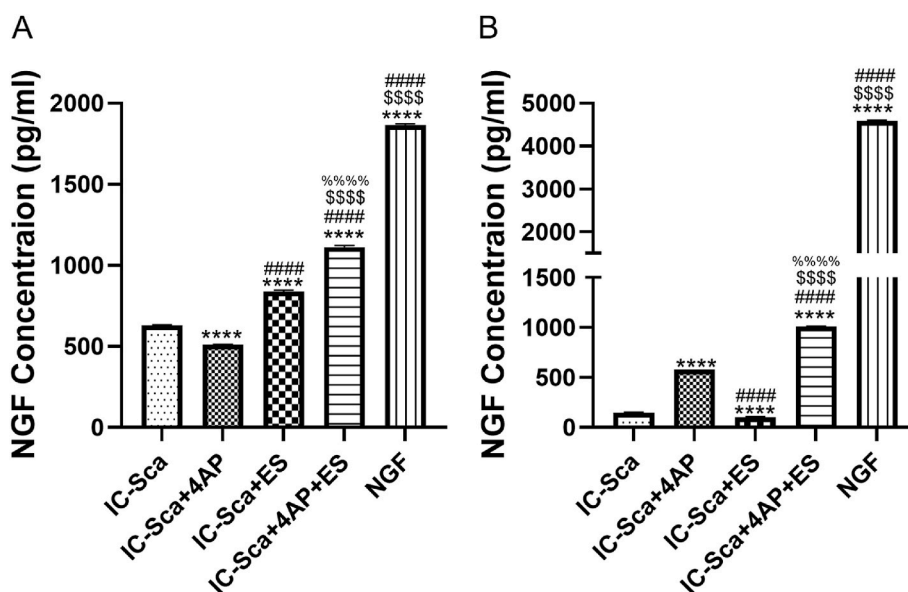


Fig. 10. Schwann cells express significantly higher amounts of NGF with combined 4-AP+ES treatment than individual 4-AP or ES treatments at days 7 and 14. Schwann cell-conditioned media collected from all treatments were quantified using NGF ELISA. NGF concentrations were measured on day (A) 7 and day (B) 14. Schwann cells treated with 100 ng/mL NGF were the positive control, while those treated with basal media were the negative control. A sample size of $n = 3$ was used for these assays, and the data is presented as Mean \pm SD. **** $p < 0.0001$ vs IC-Sca. #### $p < 0.0001$ vs IC-Sca+4-AP. \$\$\$ $p < 0.0001$ vs IC-Sca+ES. %%% $p < 0.0001$ vs NGF.

treatments displayed widespread distribution of myelinated neurons, confirming nerve regeneration. S100 β , a Schwann cell marker with higher expression during axon proliferation, was confirmed via immunostaining (Fig. 13A–ii & 13B–ii). Quantitative analysis showed significantly higher S100 β expression in the combined 4-AP+ES treatment than individual treatments, although autografts had the highest S100 β levels for both scaffold sizes (2 cm and 4 cm) (Fig. 13C & F). CD31 staining, marking endothelial cells to confirm blood vessel formation, was visible in all treated groups (Fig. 13A–iii & 13B–iii). The intensity of CD31 was significantly higher in the combined 4-AP+ES treatment compared to individual treatments and autografts (Fig. 13D & G). Additionally, the combined treatment led to significantly greater blood vessels in all treated groups than in autografts (Fig. 13E & H).

2.5.5. Neurogenic gene expressions

Regenerated nerve samples from the middle of the 4 cm scaffolds, 12 weeks post-surgery, were analyzed for the expression of neuron-specific genes (NT-3, NGF, BDNF, GDNF), neurotrophic receptors (TRKA, TRKB,

TRKC), and the angiogenic marker CD31 (Fig. 14). These genes were chosen to validate the central hypothesis outlined in Scheme 1. The TRK receptor family showed significantly higher expression in the combined 4-AP+ES stimulation than in individual treatments and autografts (Fig. 14F–H). Similarly, neurotrophic genes, including CD31, NT-3, NGF, and BDNF, were expressed at significantly higher levels in the combined treatment (Fig. 14A–D), except GDNF (Fig. 14 E), which did not follow a clear trend. These results demonstrate that the combined 4-AP+ES treatment enhances large-gap nerve regeneration by promoting angiogenesis, neurotrophic factor secretion, and elevated receptor expression (Scheme 1).

3. Discussion

Delivering growth factors or cells with scaffolds can stimulate nerve regeneration processes, but chemical and electrical stimulation may have similar and additional benefits with fewer limitations. Neurotrophins such as nerve growth factor (NGF) and BDNF can improve

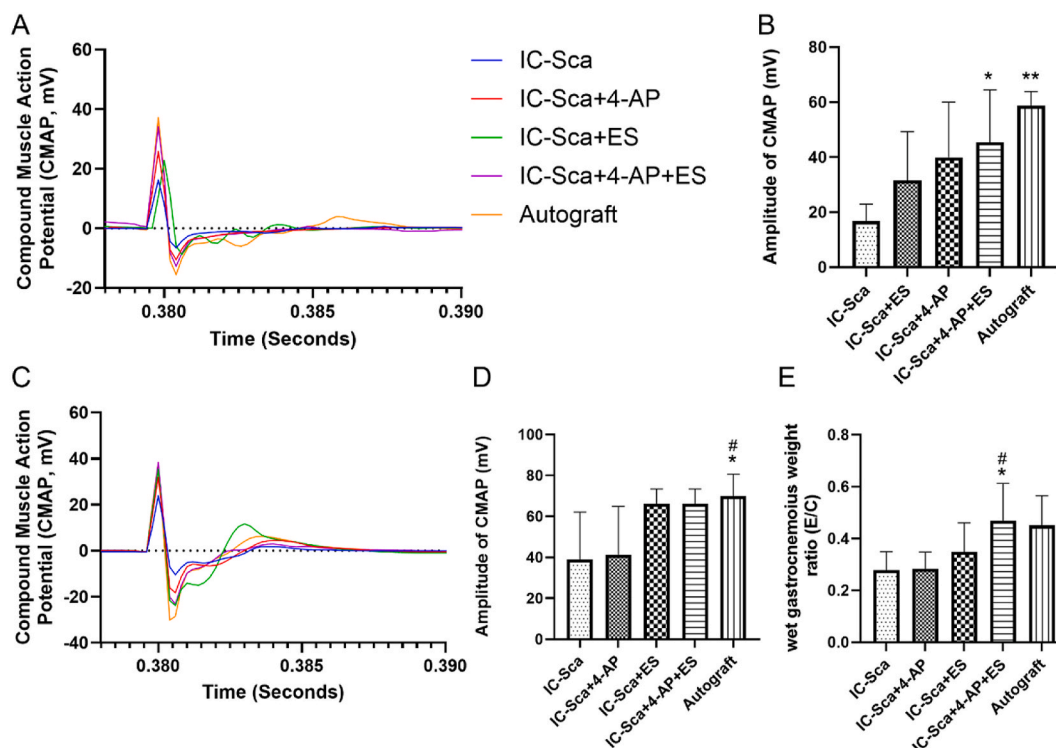


Fig. 11. The combined 4-AP+ES treatment synergistically enhances CMAP compared to individual 4-AP or ES treatments for 2 cm and 4 cm long scaffolds. (A, C) Representative CMAP traces for 2 and 4-cm long scaffolds show a second waveform across all test groups. (B, D) Quantified CMAP amplitudes for the 2 cm and 4 cm scaffolds. (E) The Gastrocnemius muscle weight ratio increased with the combined 4-AP+ES treatment, reaching levels comparable to the autograft control for 2 cm and 4 cm scaffolds (2 cm data not shown). Mean \pm SD; $n = 5\text{--}6/\text{group}$; One-way ANOVA with Tukey's multiple comparisons test; * $p < 0.05$, ** $p < 0.001$ vs IC-Sca. # $p < 0.05$ vs IC-Sca+4-AP.4.

nerve regeneration [40,41], but proteins can have high dose requirements, short half-lives, high costs, and undesired side effects [42]. Schwann cells and other neuronal support cells can also accelerate nerve regeneration, but delivering viable cells is cumbersome, costly, and requires a delivery matrix [43]. Regeneration failure in allografts has also been attributed to Schwann cell senescence [44] and lack of vasculature, so improving Schwann cell-graft interactions may improve regeneration success. However, no efforts have been made to encourage endogenous Schwann cell infiltration using a drug or other external cue to improve large-gap PNI. ES and 4-AP may accomplish this goal but will require innovative design of new polymers and delivery methods.

The benefits of electrical stimulation for muscle and nerve repair are well-established, but regenerating large nerve defects often requires biological grafts for guidance and reconstruction [45]. Recent advances have focused on conductive polymer platforms that apply localized electrical stimulation to promote tissue regeneration. Polymers like PANI, poly(3,4-ethylenedioxythiophene), and poly(pyrrole) alter their properties in response to electrical stimuli, carry charges along the tissue. They are often nondegradable, thermosetting making them difficult to process, and possess redox instability leading to a reduction in conductivity overtime [46]. Ionically conductive polymers offer a promising alternative to traditional conductive polymers by utilizing ionic conduction domains, which can be tailored for controlled electrical stimulation. This allows them to reliably modulate ion flux, membrane potential, and intracellular signaling, that in turn modulates cell functions, including adhesion, proliferation, and differentiation. Any biomedical polymer can be transformed into an IC polymer by adding ionic groups to its backbone. These ionic groups make the polymer hydrophilic, biodegradable, and erodible, allowing for reliable electrical stimulation. This stimulation activates cellular pathways that promote extracellular matrix production and vascularization, supporting tissue regeneration [47]. In this study, we chose a natural biopolymer chitosan

backbone to create IC polymers due to its relative use of chemical modification and proven biocompatibility and biodegradability.

While the ideal scaffold conductivity for tissue regeneration remains undefined, scaffolds with 10–100 μA conductivity have been shown to stimulate cells effectively [48]. Evaluating the scaffold's conductivity under physiological conditions is essential for reliable electrical stimulation in tissue engineering [49]. In our studies, unlike traditional materials such as PANI, ionically conductive polymers containing sulfonated and phytate ions maintained consistent conductivity over 12 weeks in an *in vitro* physiological environment [26]. The enhanced ionic conductivity of PA cross-linked chitosan and nerve allografts is attributed to the higher ion exchange capacity provided by the hexavalent phytate anion, which surpasses that of sulfonated chitosan. Furthermore, these IC scaffolds demonstrated consistent weight loss, maintained ionic conductivity, and preserved tensile strength over 12 weeks, making them well-suited for supporting effective nerve regeneration. Several conductive polymers including PANI, polyvinylpyrrolidone, PEDOT, polyvinylidene fluoride (PVDF) alone or in combination with metallic or carbon nanofillers including carbon nanotubes (CNTs), graphene, and demonstrate varying conductivity levels [50]. These electronically conductive scaffolds were designed to transmit applied ES and simulate damaged neural tissue tissues to provide a conducive pro-regenerative microenvironment [21,51]. For example, polydopamine/RGD-coated graphene-loaded polycaprolactone scaffolds have a conductivity of 6.37×10^{-3} S/cm [52], while CNT/sericin conduits exhibit a lower conductivity of 3.90×10^{-4} S/cm [53]. In contrast, graphene foam/polycaprolactone scaffolds show much higher conductivity at 25 S/m. The developed PA-crosslinked chitosan scaffolds reported in this study exhibited ionic conductivity (133.23 ± 4.22 mS/cm), significantly higher than many scaffolds mentioned above while addressing degradation issues. Sustained delivery of freely water-soluble molecules like 4-AP using hydrophilic chitosan-based

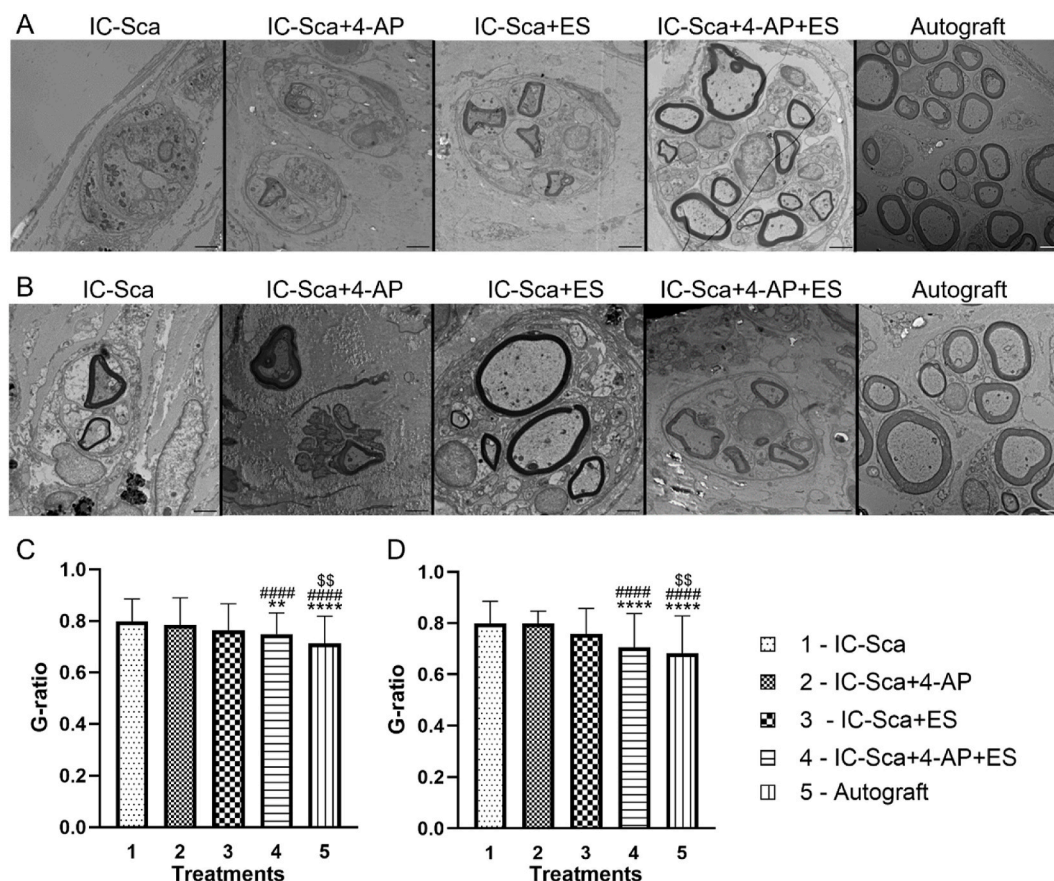


Fig. 12. Treatments 4-AP, ES, and 4-AP+ES—supported myelinated axon regeneration in 2 cm and 4 cm scaffolds at 12 weeks, with outcomes comparable to autografts. (A) TEM micrographs for 2 cm and (B) 4 cm long scaffolds, showing the mid-region cross sections of the scaffolds at 12 weeks post-surgery (Mag-1000X; Scale 10 μ m). Calculated G-ratio from TEM images for (C) 2 cm and (D) 4 cm long scaffolds. G-ratio is the inner axon diameter to outer fiber diameter ratio, where a lower ratio indicates thicker myelin. Data are expressed as mean \pm SD. n = 35 measurements per group. **p < 0.01, ****p < 0.0001 vs IC-Sca. #####p < 0.0001 vs IC-Sca+4-AP. \$\$p < 0.01 vs IC-Sca+ES.

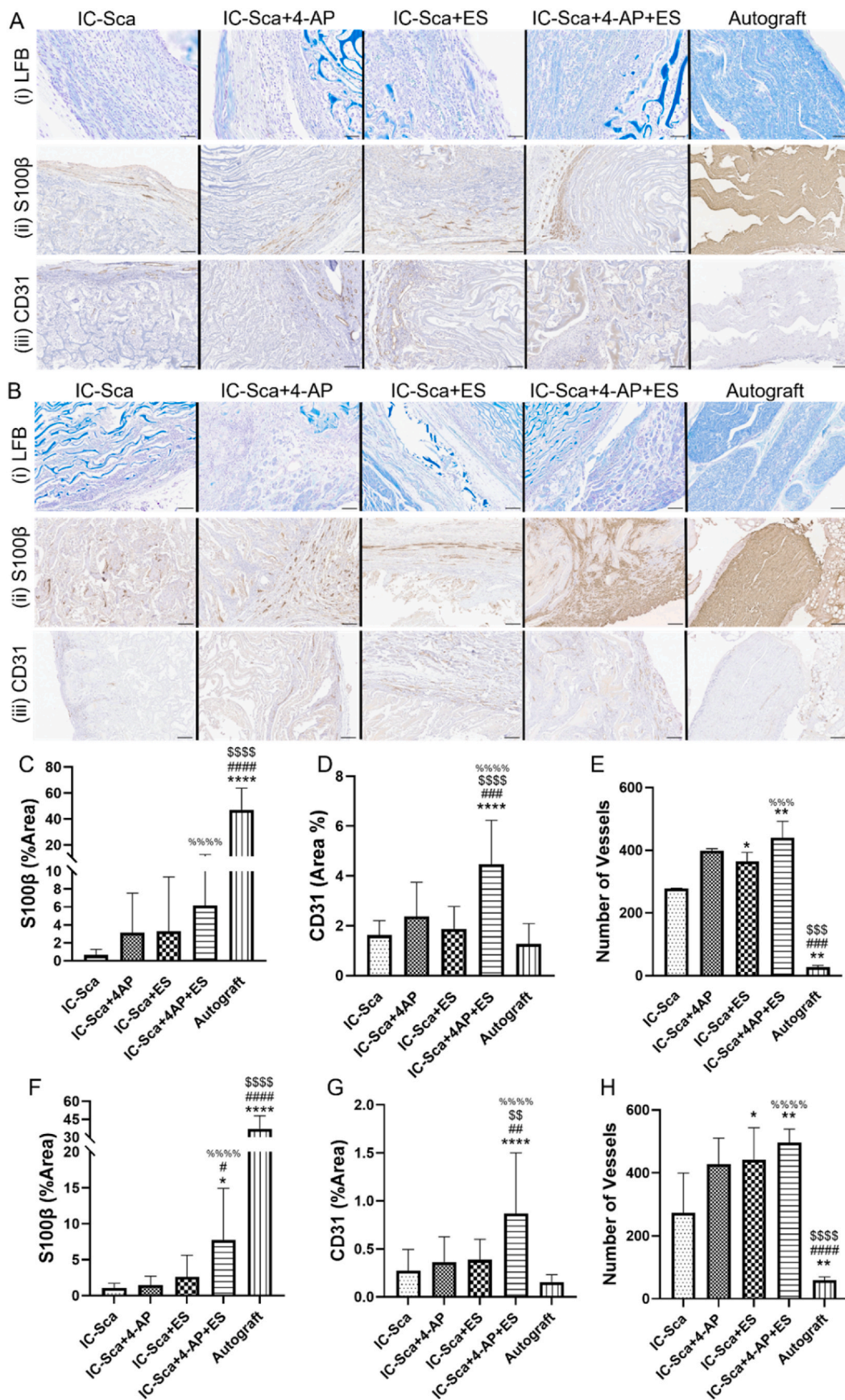
ionically conductive (IC) polymeric scaffolds presents a significant challenge. We previously reported the incorporation of 4-AP into the open lumen of halloysite nanotubes (600–900 nm) and uniformly dispersing them in an IC chitosan solution to fabricate porous scaffolds [54]. The drug-filled HNT tubes were sealed with chitosan at both ends to function as drug reservoirs, resulting in sustained 4-AP release over 7 weeks *in vitro*. In contrast, the release from allografts under similar conditions lasted only one week (data not shown). These scaffolds are kink-resistant and suturable, exhibiting acceptable suture retention strengths ranging from 18 to 20 N. The incorporation of HNT into the scaffolds enhances their stability and tensile strength by facilitating interactions between the positively charged ammonium groups of chitosan and the negatively charged surfaces of HNT [23]. The composite IC scaffolds in this maintained a constant Young's modulus over 10 weeks of degradation, indicating retention of their elastic properties due to a steady erosion rate.

Mechanical stability is essential for scaffolds to heal large nerve gaps, as it supports movement and prevents deformation. Figs. 1 and 2 show the scaffold's weight loss and corresponding tensile strength over 10 weeks. At 37 $^{\circ}$ C, the scaffolds lost approximately 10 % of their original weight while maintaining an elastic modulus between 0.75 and 0.5 MPa and tensile strength between 0.8 and 0.35 MPa in their hydrated state. The Young's modulus of the IC composite scaffold (0.58 ± 0.2 MPa) is comparable to a few clinically available small-diameter nerve guidance conduits (NeuraGen[®]: 0.08 MPa and Neuralac[®]: 0.14 MPa [55]). Adjusting the scaffold design by modifying the molecular weight of chitosan, increasing cross-link density, or incorporating nanomaterials and fibers can enhance mechanical stability [56]. This flexibility enables

the creation of robust ionically conductive (IC) scaffolds suitable for nerve repair and regeneration in higher vertebrates. For instance, IC composite scaffolds prepared for this study have tensile strength and load at break values comparable to acellular rat peripheral nerves (1.4 ± 0.29 MPa and 0.35 ± 0.14 N), making them mechanically stable and suitable for implantation in nerve defects. Most nerve conduits made from natural and synthetic polymers provide similar mechanical strength, but this can be adjusted by creating composites [57,58].

A series of *in vitro* experiments were conducted to investigate the adhesion, viability, proliferation, neurite outgrowth, neurotrophic protein, and gene expressions in the rat Schwann, PC-12 and F11 cells to examine the individual and combined effects of chemical (4-AP) and electrical stimuli, comprehending their bioactivity during regeneration. Results suggested that the combined treatment of 4-AP (from chitosan composites) and electrical stimulation in both neuronal (PC-12 & F-11) and glial cells (Schwann cells) showed adequate cell-scaffold interactions with prominent neurite extensions. Higher expression of neurotrophic proteins, their genes (such as MPZ, NGF, BDNF, GDNF, NT-3, NT-4, S100b) and Trk receptors (Trk A, Trk B and Trk C) in Schwann cells at longer time points stimulate axon regeneration with myelin sheath formation. These results are in line with previously published reports, which demonstrated the proliferation and differentiation with the expression of neuron-specific proteins and genes.

The ability to control localized physical and chemical signals with these scaffolds allows for extended treatment periods, enhancing motor function recovery that is unattainable with short-term interventions. Scheme 1 illustrates our novel approach, which significantly improves peripheral nerve regeneration through the synergistic application of 4-



(caption on next page)

Fig. 13. The combined 4-AP+ES treatment synergistically enhances myelin sheath and blood vessel formation compared to individual 4-AP or ES treatments in the regenerated nerve for 2 cm and 4 cm long scaffolds. (A, B) (i)LFB Luxol Fast Blue staining for myelinated nerves (scale bars = 200 μm). (A, B) (ii) S100β immunostaining for Schwann cell activity (scale bars = 100 μm). (A, B) (iii) CD31 immunostaining for endothelial cell marker (scale bars = 100 μm). Image intensity quantification (C, F) S100β, (D, G) CD31, and (E, H) number of blood vessels. Blood vessels were counted N = 12 sections/Sample manually). One-way ANOVA with Dunnett’s multiple comparisons test. ****p < 0.0001; and (E) Quantification of CD31 immunostaining in terms of percentage of area stained. N = 10-12 sections. One-way ANOVA with Tukey’s multiple comparisons test. *p < 0.05, **p < 0.01, ****p < 0.0001 vs IC-Sca. ###p < 0.001, ####p < 0.0001 vs IC-Sca+4-AP. \$\$\$p < 0.001, \$\$\$\$p < 0.0001 vs IC-Sca+ES. %p < 0.05, %%%p < 0.001 vs autograft.

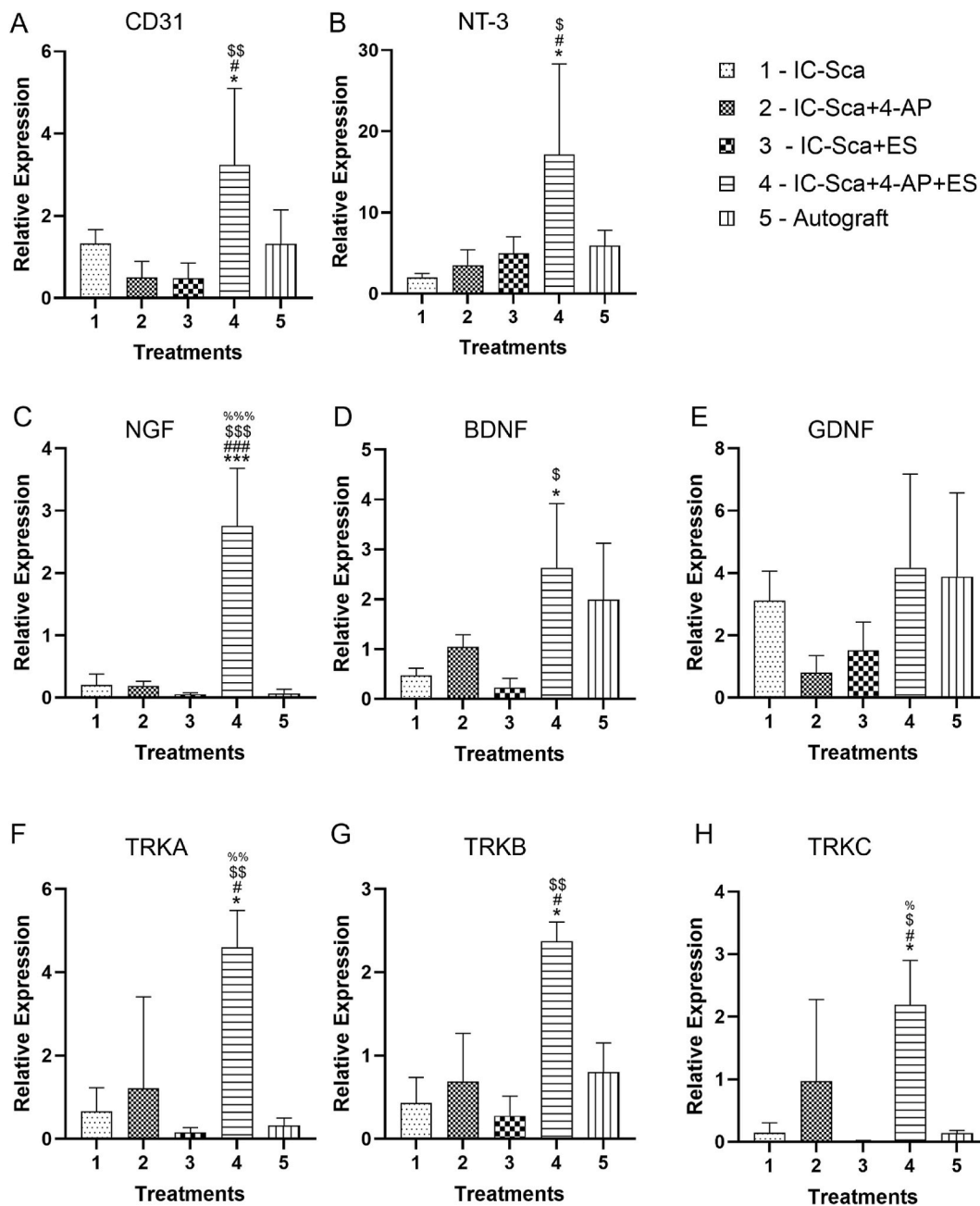


Fig. 14. Regenerated nerve samples from the 4 cm scaffolds showed significantly higher neurotrophic and endothelial marker gene expression under the combined 4-AP+ES treatment than individual 4-AP or ES treatments. (A–H) At 12 weeks post-injury, 4-AP+ES treatment significantly upregulated neurotrophic factors (NGF, BDNF, GDNF & NT3) and their receptors (TRKA, TRKB & TRKC) and endothelial marker (CD31) compared to other groups. Data are Mean ± SD; n = 3–4. One-way ANOVA with Tukey’s multiple comparisons test. *p < 0.05, ***p < 0.001 vs IC-Sca. #p < 0.05, ###p < 0.001 vs IC-Sca+4-AP. \$p < 0.05, \$\$p < 0.01, \$\$\$p < 0.001 vs IC-Sca+ES. %p < 0.05, %%%p < 0.001 vs autograft.

AP and electrical stimulation (ES), facilitated by a bioengineered scaffold with sustained ionic conductivity and controlled chemical release properties. We previously reported that Schwann cells secrete important neurotrophic factors in response to 4-AP dosage, and the sustained

release from scaffolds further promoted nerve regeneration in critical-sized sciatic nerve defects, achieving comparable sciatic functional index (SFI) outcomes to autograft treatment. Numerous studies have demonstrated the efficacy of 4-AP and ES in promoting nerve

regeneration and functional recovery following crush injuries. The localized delivery of 30 or 60 μg of 4-AP at the repair site results in concentrations too low for systemic detection. Extensive prior studies, including our previous study, have shown this optimized dose to be non-toxic. This dosage is significantly below toxic levels reported by the U. S. Environmental Protection Agency (EPA). Furthermore, studies in animals such as rodents and dogs, summarized by the EPA and NCI, showed no adverse effects on body weight or blood cell counts at much higher doses (1–5 mg/kg/day) [59–61]. Our findings align with previous reports on the regulatory effects of both 4-AP and ES on Schwann cells and neurotrophic factor secretion *in vitro* and during sciatic nerve regeneration. However, the synergistic effects of 4-AP and ES, coupled with engineered delivery properties, in healing larger sciatic nerve defects have not been extensively characterized.

We are the first to evaluate the efficacy of an IC polymeric composite scaffold for repairing critical-sized sciatic nerve defects (1–5 cm) in rats, using a 2 cm scaffold and a 4 cm looped scaffold to mimic clinical conditions and study the synergistic effect of 4-AP and ES on nerve healing. We modeled our 4 cm scaffold implantation after a 1 cm sciatic nerve defect in Lewis rats, using a 4 cm reversed isograft (biological graft) looped around the biceps femoris muscle, similar to our study design. This study showed that the looped configuration of implanted nerve grafts did not hinder nerve regrowth and resulted in an adequate number of myelinated fibers after 12 weeks. The creation of clinically relevant >4 cm defects in a rat model is technically not feasible. Our proposed overall approach is not yet mature for translation. Therefore, we conducted *ex vivo* and *in vivo* experiments to address scaffold physicochemical properties, electrical conductivity, dose-dependent factor release, and nerve regeneration as detailed in the manuscript. These studies lay the foundation for translational work using larger, >4 cm long nerve gaps in higher vertebrates in the future. Therefore, we based our 4 cm long scaffold implantation in the loop fashion in rat model as published in the literatures [62]. In addition, we believe that the ionically conductive nature of the scaffold and the loop structure may also contribute to the observed CMAP measurements. The higher CMAP amplitude in the 4 cm scaffold may result from additional depolarization volleys transmitted through the scaffold by muscle bundles as well [63, 64]. This likely represents a burst of simultaneous or rapidly sequential nerve impulses passing to an end organ, synapse, or neural center [65]. These findings suggested that enhanced electrical activity and neural responsiveness were facilitated by the ionically conductive scaffold.

The Trk family receptors (TrkA, TrkB, and TrkC) and neurotrophic factors, such as NGF, BDNF, NT-3, and GDNF, are critical players in nerve regeneration. These factors support neuronal survival, promote axonal growth, and facilitate functional recovery following nerve injuries [38]. Spatiotemporal expression of neurotrophic factors is crucial at different stages of axon regeneration. NGF and NT-3 are upregulated shortly after an injury to initiate axonal sprouting, while BDNF and GDNF play a role in sustaining axonal growth and remyelination in the later phases. The chronological expression of the above neurotrophic factors was tested and quantified via gene expression, immunostaining, and series protein assays using *in vitro* and *in vivo*-derived samples. The relationship between the Trk pathway and K^+ channel blockers significantly enhance nerve regeneration through a synergistic mechanism. The K^+ channel blocker 4-AP extends neuronal depolarization, which enhances neurotransmitter release and increases neuronal firing. By prolonging neuronal depolarization, 4-AP contributes to improved nerve regeneration [66]. Normally, potassium channels facilitate the exit of K^+ ions from neurons, aiding in the repolarization of the cell after an action potential. When these channels are blocked, the depolarized state of the neurons is prolonged, which increases neurotransmitter release and sustains neuronal excitability [66]. This process elevates neurotrophic factors like NGF and BDNF secretion, activating Trk receptors and triggering intracellular signaling through the PI3K/Akt and MAPK/ERK pathways—key for axon growth, neuronal survival, and synaptic plasticity [67]. Prolonged depolarization further enhances neuron

sensitivity to these factors, amplifying TrkA and TrkB receptor activation, which promotes axon repair and regeneration. The ES has emerged as a valuable approach to enhance the effects of these neurotrophic factors and their respective Trk receptors, providing a multifaceted strategy for accelerating nerve repair [68]. ES has been demonstrated to boost endogenous neurotrophic factor levels while enhancing the expression of Trk receptors, which play a critical role in promoting axonal regeneration. For instance, ES has been shown to upregulate BDNF and its receptor TrkB, leading to faster axonal growth and improved functional recovery in animal studies and clinical applications.

Electrical stimulation (ES) can increase NGF expression, supporting early axonal growth and guidance. It promotes neurotrophic factor release and enhances their binding to Trk receptors, amplifying the downstream signaling essential for axonal growth and repair. When combined with 4-AP, ES further boosts neurotrophic factor release, aiding remyelination and restoring nerve conduction. This dual treatment increases the expression of TrkA, TrkB, TrkC, and factors like NGF, NT-3, and BDNF, promoting regeneration at various stages. K^+ channel blockers like 4-AP amplify the Trk pathway's effects, enhancing synaptic activity and creating better conditions for nerve repair. Additionally, ES supports vascularization, aiding in nutrient delivery and waste removal, which are critical for sustained nerve health and functional recovery. It also contributes to immune responses that foster a favorable repair environment. Together, ES and 4-AP form a powerful combination for nerve regeneration, leveraging neurotrophic factor-driven pathways and vascular support to maximize functional recovery.

4. Conclusion

This study demonstrated the effectiveness of an ionically conductive chitosan-based nerve conduit platform for delivering 4-aminopyridine and electrical stimulation to treat large nerve defects. The scaffolds, featuring aligned micropores, guided axonal growth while ensuring sustained 4-AP release and ES delivery. Additionally, they maintained mechanical stability and exhibited controlled degradation, both crucial for large-gap nerve repair. These IC scaffolds supported Schwann cell attachment, proliferation, and neurotrophic factor secretion *in vitro*. The secretion of neurotrophic factors and their receptors by Schwann cells under combined ES and 4-AP treatment was significantly higher than with 4-AP or ES alone, confirmed at both gene and protein levels. The efficacy of the IC polymeric composite scaffold was evaluated in critical-sized sciatic nerve defects (1–5 cm) in rats, using both 2 cm and 4 cm looped scaffolds to mimic clinical conditions. The combined 4-AP+ES treatment improved nerve healing, as shown by electrophysiology and histology, with significantly higher compound muscle action potential (CMAP) amplitudes than individual treatments. The results were comparable to autografts, indicating a synergistic effect on functional recovery. Both short (2 cm) and long (4 cm) nerve defects showed thick myelination and axon regeneration at 12 weeks post-surgery in the 4-AP+ES group, with outcomes similar to autografts. The combined treatment also enhanced myelin sheath expression and neovascularization, with elevated levels of neurotrophic genes (NGF, NT-3, BDNF, GDNF), their receptors (TRKA, TRKB, TRKC), and the endothelial marker CD31. These findings suggest that the combined delivery of 4-AP and ES using the IC scaffold accelerates large-gap nerve regeneration, achieving results comparable or superior to autografts. This approach may also apply to other electroactive tissues, such as muscle, and broader regenerative medicine applications.

5. Methods

5.1. Materials

High molecular weight chitosan was obtained from Tidal Vision (Bellingham, WA). Glacial acetic acid, sodium hydroxide pellets,

phosphate-buffered saline (PBS), LIVE/DEAD™ Viability/Cytotoxicity Kit, regenerated cellulose dialysis tubing with an MWCO of 3500 Da, 4 % Paraformaldehyde solution, Triton™ X-100, and NucBlue DAPI reagent were purchased from Fisher Scientific (Fair Lawn, NJ). 4-Aminopyridine (4-AP) was sourced from Alomone Labs (Jerusalem, Israel). Halloysite nanoclay tubes (HNTs) for 4-AP loading, papain, glutaraldehyde, other salts, and analytical grade solvents were acquired from Sigma Aldrich (St. Louis, MO). Dulbecco's minimum essential medium (DMEM) media from Lonza Bioscience (Morrisville, NC). All cell culture supplies including pen-strep (P/S), fetal bovine serum (FBS), cell culture plates (Falcon brand), 0.25 % trypsin EDTA, Quant-iT™ PicoGreen™ dsDNA Assay Kit, and Cell Titer 96® AQueous One Solution Cell Proliferation Assay, and Vicryl® sutures were purchased from Fisher Scientific (Fair Lawn, NJ). Modified porcine trypsin protease and Cell Titer 96® AQueous One solution cell proliferation assay were purchased from Promega, Madison, WA. QIAzol Lysis Reagent and RNeasy Plus Mini kit were purchased from QIAGEN Inc. (Germantown, MD), while iScript cDNA Synthesis Kit and iTaq Universal SYBR Green Supermix were purchased from Bio-Rad (Hercules, CA). Normal goat serum, anti-NGF antibody (catalog #ab6199), anti-MPZ antibody (catalog #ab61851), anti-BDNF antibody (catalog #ab108319), anti-S100b (catalog #ab52642) and goat anti-rabbit Texas Red (catalog #ab6719) were purchased from Abcam (Cambridge, MA). Rat Schwann cells (cell line RSC96) were purchased from ATCC (Manassas, VA). PC-12 cells. Transmission electron microscopy supplies, including resin, uranyl acetate 1 %, embedding molds, osmium tetroxide, propylene oxide, and 0.2 mM cacodylate buffer, were purchased from Electron Microscopy Sciences (Hatfield, PA). Phytic acid was sourced from TCI America (Portland, OR). S100B, CD31, and Neurofilament-H (NF-H) antibodies were purchased from Cell Signaling Technology (Beverly, MA). All surgical tools were purchased from Fine Science Tools (Foster City, CA).

5.2. Scaffold preparation and characterization

5.2.1. Drug loading

To load 4-AP into halloysite nanotubes (HNTs), we followed our previously reported protocol [23]. A saturated solution of 4-AP was prepared by dissolving the drug in ultrapure distilled water (50 mg/mL) at room temperature. HNT dry powder was then added to this solution (1:2 w/w) and ultrasonicated for 1 h to ensure proper dispersion and prevent precipitation. Cyclic vacuum pumping replaced the air inside the HNTs with the drug solution. The vacuum process was applied for 30 min and repeated thrice before leaving it under vacuum overnight for enhanced loading. The HNT/4-AP powder was separated by centrifugation (5000 rpm, 20 min), washed with distilled water three times, and freeze-dried for 24 h to obtain the final HNT/4-AP dry powder.

5.2.2. Scaffold fabrication

A 3 wt% chitosan solution in 2 % glacial acetic acid was mixed with 5 wt% HNT containing 4-aminopyridine and homogenized. Two milliliters of this solution were poured into tubes (5.75 mm inner diameter, 60 mm height) positioned vertically in a metal base mold. The mold was immersed in liquid nitrogen for unidirectional freezing for 20–30 min as per our published work [23]. After freezing, the tubes were freeze-dried overnight and crosslinked with phytic acid (PA) to introduce phytate ions. The freeze-dried samples were treated with 1 N sodium hydroxide, immediately washed with ethanol to remove salts, and incubated in 2 % PA for 1 min. Finally, they were washed with deionized water to remove unbound PA. Thin wafer scaffolds for *in vitro* studies were also prepared to fit 6- or 24-well plates.

5.2.3. Ionic conductivity

The conductivity of the various IC polymers and chitosan scaffolds cross-linked with phytic acid, sulfuric acid, and epichlorohydrin were measured [19,23]. The resistance of rectangular (10 mm × 20 mm) scaffolds in PBS (pH 7.4 at 37°) was measured using a CHI 760E

bipotentiostat (Austin, TX). The conductivity of the scaffold was calculated using $R = (\rho * L) / s$ and $\kappa = 1 / \rho$, where R is the measured resistance, L is the length of the test sample, and S is the cross-sectional area of the test sample. ρ and κ represent the resistivity and conductivity, respectively. A sample size of $n = 4$ was used for all these measurements, and the data was expressed in mean ± standard deviation (SD).

5.2.4. Drug release studies

In vitro drug release studies were conducted as described in our previous work [23]. The study groups included uncross-linked (Sca+4-AP and Sca+HNT+4-AP) and their cross-linked scaffolds (IC-Sca+4-AP and IC-Sca+HNT+4-AP). Scaffolds of each type ($n = 5$) were placed in a cellulose dialysis bag with 1 mL of PBS and suspended 10 mL PBS in glass vials maintained at 37 °C in an orbital shaker (Isotemp SWB 27, Thermo Fisher Scientific, Waltham, MA, USA). A 1 mL of the released media at various time points was collected, and 4-AP concentrations were measured using UV-Vis spectroscopy (Genesys 150, Thermo Fisher Scientific, Waltham, MA, USA) at 262 nm [23].

5.2.5. Degradation analysis

Scaffolds ($n = 5$) were incubated in 10 mL PBS in glass vials and subjected to degradation at 37 °C (physiological) and 55 °C (accelerated) in a shaking water bath incubator. At 3, 6, and 10 weeks, samples were washed with DI water to remove PBS and vacuum-dried overnight. The % weight loss was calculated using the formula: $(W_0 - W_t) / W_0 \times 100$, where W_0 is the initial weight and W_t is the weight at the given time point.

5.2.6. Mechanical testing

Scaffolds ($n = 5$) subjected to degradation in PBS at 37 °C and 55 °C were collected at 0, 3, 6, and 10 weeks and subjected to tensile testing using an 858 Mini Bionix II servohydraulic testing system (MTS, Eden Prairie, MN, USA) at a ramp speed of 5 mm/min until failure. Young modulus, ultimate strength, and load at break were calculated from the stress-strain curve.

5.2.7. Biocompatibility assessment

The biocompatibility of IC scaffolds with different 4-AP, ES, and combined 4-AP/ES treatments was tested using a subcutaneous implantation model in 15 Wistar rats (200–250g, Charles River Laboratories, Wilmington, MA). The rats were divided into five groups: Sca (chitosan), IC-Sca, IC-Sca+4-AP, IC-Sca+ES, and IC-Sca+4-AP+ES. Each rat was anesthetized with isoflurane (3 %) and implanted with two scaffolds. A 2.5 cm incision was made on the dorsal side, creating a subcutaneous pouch for individual scaffolds (8 × 2 mm) implantation. Blood samples from tail veins were collected at 3-, 7-, and 14-days post-surgery to analyze IL-6 and IL-10 cytokines by ELISA kits (R&D system, Inc. Minneapolis, MN) [69]. After two weeks post-implantation, the rats were sacrificed using carbon dioxide overdose, and scaffolds ($n = 6$) of each type were removed and collected for evaluation.

5.3. *In vitro* cell culture

5.3.1. *In vitro* culture of schwann cells (SCs)

Rat Schwann cells (SCs, RSC96) were used to study scaffold interaction under 4-AP, ES, and 4AP/ES stimulations. Per the standard protocols, scaffolds were sterilized by incubation in 70 % ethanol and exposure to UV light in a tissue culture hood. These scaffolds were incubated with Dulbecco's Modified Eagle's Medium (DMEM) supplemented with 5 % Fetal Bovine Serum (FBS) and 1 % Penstrep (P/S) in an incubator (37 °C, 5 % CO₂) overnight. Media was aspirated, and 3000 Schwann cells/scaffold ($n = 5$) were seeded for the *in vitro* experiments. Cell culture media changes changed every alternative day. Likewise, ES was also applied every alternative day using a culture pacing system (Ion Optix, Westwood, MA), which has a C-dish electrode system that fits tightly into each well of the 24-well plate. The applied stimulation

parameters were 1 V and a frequency of 20 Hz for 20 min inside the incubator. Our studies showed that a relatively low voltage range of 0.5–1.0 V is sufficient to trigger cellular responses. Additionally, a frequency of 20 Hz mimics the natural firing rate of neurons, and a minimum of 20 min stimulation did not cause any chronic stress [25].

5.3.2. *In vitro* bioactivity assessment using neuronal cell lines

The pheochromocytoma PC-12 and F11 cells were used to study the neurite outgrowth by cultured Schwann cells under different treatments (conditioned media). The cells were seeded at a density of 10,000 in chamber palates and treated with 750 μ L DMEM media (2 mM L-Glutamine, 1 % PS, 1 % FBS) + 250 μ L of conditioned media to assess the neurite extension over 5 days. Likewise, PC-12 cells at a density of 10,000 were cultured on poly-L-lysine coated TCPS plates using RPMI media supplemented with 1 % PS, 5 % FBS, and 10 % Horse Serum (HS) + 250 μ L of conditioned media to assess the neurite extension over 7 days [70]. Likewise, PC-12 cells at a density of 10,000 were cultured on poly-L-lysine-coated TCPS plates using 250 μ L RPMI media supplemented with 1 % PS, 5 % FBS, and 10 % Horse Serum (HS) + 250 μ L of conditioned media to assess the neurite extension over 7 days. Positive control included 100 ng/mL of NGF to compare the findings. Following the manufacturer's protocol, cells were stained using the Neurite Outgrowth Staining Kit (Invitrogen). After applying the cell viability indicator, membrane stain, and background suppression dyes, cells were imaged with a confocal microscope (Zeiss LSM 880). The mean length of the neurite extensions was measured from the cell body to the farthest neurite branch and were quantified using ImageJ software [71].

5.3.3. Cell adhesion and morphology

The surface morphology of SCs on scaffolds was imaged on a scanning electron microscope (SEM) (JEOL JSM-6335F, JEOL USA, Inc., MA, USA). Before imaging, scaffolds with cells were fixed in a 3 % glutaraldehyde solution and coated with Au/Pd using a Polaron E5100 sputtering system (Quorum Technologies, East Sussex, UK) [23]. Images were then processed and analyzed using ImageJ software (NIH, Bethesda, MD).

5.3.4. Cell viability and proliferation

The Schwann cell viability on scaffolds under different treatments was assessed using a live/dead assay with the Live/dead™ Viability/Cytotoxicity Kit (Invitrogen, Waltham, MA). In brief, 3-, 7-, 14-, and 21-days post-culture scaffolds (n = 5/group) were stained per the manufacturer's protocol. Confocal microscopy (Zeiss LSM 880, Carl Zeiss AG, Oberkochen, Germany) was used for imaging, and images were processed with ImageJ (NIH, Bethesda, MD). Tissue culture polystyrene (TCPS) surface was used as a control.

The metabolic activity of cultured cells under various treatments was measured using a Cell Titer 96® Aqueous One solution cell proliferation assay. In brief, scaffolds (n = 5/group) were washed with PBS at 1-, 3-, and 7-days post-culture, then incubated with fresh serum-free media and MTS reagent per the manufacturer's protocol for 2 h. The absorbance or color intensity of the reaction media was immediately read at 490 nm on a plate reader (Biotek, Synergy HTX, Agilent Technologies, CA).

5.3.5. Neurotrophic protein expression

Neurotrophic protein expression in Schwann cells on IC scaffolds under various treatments was analyzed using immunohistochemistry and proteomics. BDNF, NGF, and MPZ were stained in 14-day cultured scaffolds. After fixation with 4 % paraformaldehyde and permeabilization with 0.2 % Triton X-100, scaffolds were blocked with 10 % goat serum and incubated with primary antibodies (anti-NGF, anti-MPZ, anti-BDNF) overnight. Secondary antibodies (Texas Red) were applied for 1 h, followed by DAPI staining. Confocal microscope images (n = 15) were processed using ImageJ, and immunofluorescence was quantified as total corrected cell fluorescence (TCCF) [23].

Proteomic analysis was conducted to quantify neurotrophic factors

secreted by Schwann cells under various treatments. Conditioned media from IC-Sca, IC-Sca+4-AP, IC-Sca+ES, IC-Sca+4-AP+ES, NGF-treated cells (positive control), and TCPS (negative control) at day 14 were analyzed. The media was reduced with 5 mM dithiothreitol for 90 min, alkylated with 10 mM iodoacetamide for 1 h in the dark, and digested with porcine trypsin protease overnight. Peptides were desalted, dried, and resuspended in 0.1 % formic acid. Absorbance at 280 nm was used to normalize the total peptide injection amount across samples. Samples were analyzed using a Thermo Scientific Ultimate 3000 RSLCnano UPLC system coupled to a Thermo Scientific Eclipse Tribrid Orbitrap mass spectrometer. Each sample was injected onto a nanoEase M/Z Peptide BEH C18 column and separated using reversed-phase UPLC with a gradient of 4–30 % Solvent B over 50 min at 300 nL/min, followed by a 30–90 % ramp over 10 min. Peptides were eluted into the mass spectrometer using positive-mode electrospray ionization. MS1 scans were recorded at 120,000 resolution, followed by data-dependent MS2 scans at 15,000 resolution for ions above a 5.0e4 intensity threshold. Dynamic exclusion was set for 30 s after one observation.

Peptides were identified and quantified using MaxQuant software (v2.0.2.0) with the Andromeda search engine and label-free quantification. Raw data were searched against the UniProt Rattus Norvegicus reference proteome and the MaxQuant contaminants database. The minimum peptide length was set to 5 residues, with a maximum mass of 4600 Da, and up to 5 variable modifications, including Met oxidation, N-terminal acetylation, and deamidation. Carbamidomethylation of Cys was fixed, and trypsin/P was specified with a maximum of 2 missed cleavages. A 1 % false discovery rate was applied to peptides and proteins. Results were visualized in Scaffold software.

5.3.6. *In vitro* and *In vivo* sample analysis for neurotrophic gene expression

Neurotrophic gene expression in Schwann cells under various treatments was analyzed using qPCR, with an NGF-treated group as a control. The primer sequences are listed in Table 1. Schwann cells (2000 cells per scaffold, n = 6 per group) were cultured for 14 days. RNA was extracted at 7 and 14 days using the RNeasy Plus Mini Kit and QIAzol/chloroform extraction. After adding 900 μ L QIAzol, samples were stored at -80° C. Chloroform was added, followed by centrifugation, and the RNA layer was purified with ethanol and RNeasy spin columns. NanoDrop assessed RNA quality and quantity. RNA (500 ng) was reverse transcribed, and PCR was performed using iTaq SYBR green on a BioRad CFX96 machine. Likewise, regenerated axon samples from rats with a 4-cm long-gap defect were subjected to neurotrophic gene analysis. The delta-delta method was used to analyze and normalize relative gene expression with the beta-actin (β -Act) housekeeping gene [72].

5.3.7. Neurotrophic protein secretion- western blot analysis

Schwann cell-secreted neurotrophic proteins on scaffolds under different treatments were measured using a western blot following published protocols [73]. After 14 days of culture, cells were scraped into RIPA buffer, vortexed, and centrifuged at 12,000 rpm for 20 min at 4 $^{\circ}$ C. The supernatant was mixed with Laemmli buffer, boiled at 70 $^{\circ}$ C for 10 min, and run on SDS-PAGE gels. Proteins were transferred to PVDF membranes, blocked with 5 % milk in TBS-T for 5 h, and incubated with primary antibodies (anti-NGF, anti-S100 β , and anti-BDNF) [74]. After washing, secondary antibodies were added, and chemiluminescence detection was performed using Pierce ECL [75]. Images were analyzed with ImageJ.

5.3.8. Neurotrophic protein secretion - ELISA analysis

The secretion of NGF from Schwann cells was measured using a commercial ELISA Kit (RayBio, Peachtree Corners, GA) according to the manufacturer's instructions. Detection through proteomics was unsuccessful due to interference from bovine FBS peptides used in cell culture. Schwann cells were cultured in FBS-free media one day before collecting conditioned media for quantification. Media samples collected on days 3, 7, and 14 post-seeding were used to measure NGF levels [76].

Table 1
List of neurogenic primers used.

Genes	Forward Primer	Reverse Primer	Ref
NGF	AAGGACGCAGCTTCTATCC	CTATCTGTGTACGGTCTGCC	[80]
BDNF	TACCTGGATGCCGCAAACAT	TGGCCTTTTGATACCGGGAC	[81]
GDNF	AGACCGGATCCGAGGTGC	TCGAGAAGCCTCTTACCGGC	
NT3	CACCCAGAGAACCAGAGCAG	TCTGAAGTCAGTGCTCGGAC	[82]
NT4	CCCTGCGTCAGTACTTCTCGAGAC	CTGGACGTCAGGCACGGCCTGTTC	[83]
CD31	GCCGTCAAATACTGGGTTAGT	GCACTGTACACCTCCAAAGAT	[84]
TRKA	TGGTGCTTCGCCCTCAACCAG	ATGGTGACACAGGTATCACTG	[85]
TRKB	ATTGACCCAGAGAACATCAC	CAGGAAATGGTCAACAGACT	
TRKC	CCCTACACCTCCTATCACTG	CTGAAATCCTTCTGGCAG	
S100B	GCCCTATTGATGCTTCCACC	GAACTCATGGCAGGCCGTGGTC	[86]
b-Actin	GCAAGTGCTTCTAGCGGACTG	CTGCTGTACCTTACCCTTCC	[87]

5.4. In vivo long-gap nerve regeneration assessments

5.4.1. Animal model

Forty Wistar rats (200–250g, male and female, Charles River Laboratories, Wilmington, MA) were randomly assigned to five groups: autograft, IC-Sca, IC-Sca+4-AP, IC-Sca+ES, and IC-Sca+4-AP+ES. The rats had free access to food and water in a temperature-controlled room with a 12-h light/dark cycle. They were acclimatized for one week before surgery and were cared for according to the guidelines approved by the Institutional Animal Care and Use Committee (IACUC) at the University of Connecticut.

5.4.2. Surgical procedure

Animals were anesthetized with 2.5 % isoflurane and oxygen. The right hind limb was shaved and cleaned with betadine and alcohol. Body temperature was maintained at around 37 °C using a warming pad. Under aseptic conditions, a 30 mm skin incision was made to expose the right sciatic nerve through a gluteal muscle split, per our prior published work. A 20 mm nerve segment was removed, and for small-gap defects, 2 cm IC chitosan conduits were secured to the nerve stumps with 8–0 nylon sutures (Suppl. Figs. 4 and 5). For autograft groups, the transected segment was reversed and sutured back. For the 2 cm nerve defect, a 4 cm scaffold was implanted in a loop configuration, following previously published methods, to simulate a more challenging and clinically relevant defect size. Muscle and skin incisions were closed with 5–0 Vicryl sutures. Post-surgery, animals were monitored for behavioral changes and managed for pain with buprenorphine and meloxicam. A saturated 1.3 % picric acid solution was applied to the denervated foot to prevent self-mutilation. After twelve weeks, animals were euthanized using CO₂ asphyxiation.

5.4.3. Electrical stimulation

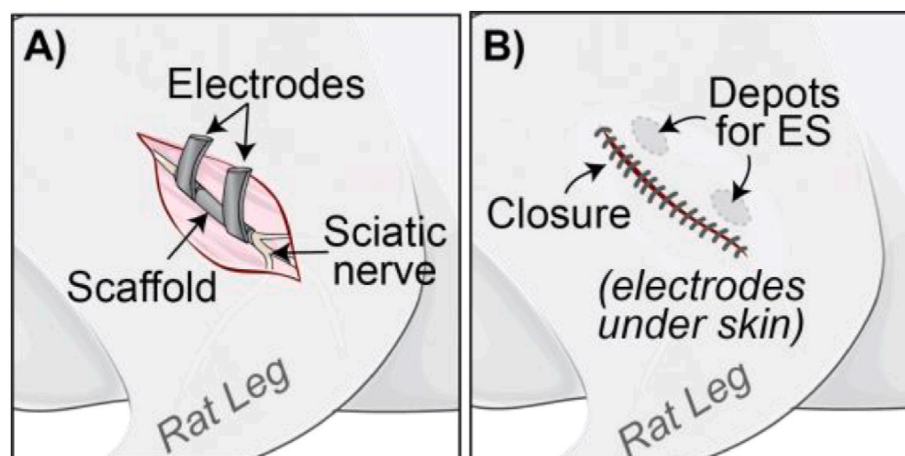
Rats were anesthetized with isoflurane before electrical stimulation (ES). Scheme 2 illustrates the percutaneous application of ES using implanted ionically conductive electrodes. Patch electrodes from a commercial TENS unit (LG TEC Elite, LSI International, St. Louis, MO) were placed on the rats' backs, with the implanted electrodes buried under the skin. The ES parameters included a current of 2 mA and a frequency of 20 Hz, applied for 20 min every three days.

5.4.4. Electrophysiological measurements

Electrophysiology measurements were conducted following the established protocols on the anesthetized rats [77]. The hair on the operated hind limb was shaved, and the rats were placed on a warming pad to maintain body temperature. The hind limb was extended, and the paw was secured with surgical tape for electrode access. A stimulating electrode was placed 5 mm deep subcutaneously on either side of the sciatic notch, about 2 cm apart. The recording electrode was aligned with the gastrocnemius muscle. In contrast, the reference electrode was positioned next to the Achilles tendon at a 30° angle, and the grounding electrode was attached to the tail. Recordings were taken 12 weeks post-surgery using a Biopac MP36 (Biopac Systems Inc, Goleta, CA) with 10 V electric stimulation and a 5 Hz sampling rate. The compound muscle action potential (CMAP) was recorded to assess functional recovery and reinnervation, analyzed with Biopac Student Lab software (version 4.1.6), and plotted using GraphPad Prism 10, represented as the peak-to-peak amplitude of the biphasic wave.

5.4.5. Gastrocnemius muscle weight analysis

Twelve weeks post-surgery, animals with short-gap (2 cm) and long-gap (4 cm) defects were sacrificed to remove the gastrocnemius muscle from the right (experimental, E) and left (contralateral, C) hind limbs. The wet weight of the gastrocnemius muscles was measured using a



Schematic 2. (A) Schematic of surgery with electrode wrapped around the implanted scaffold, and (B) showing closure with electrodes under the skin.

weighing balance. The muscle weight ratio was calculated by dividing the experimental limb's weight by that of the contralateral limb to assess muscle atrophy [78].

5.4.6. Transmission electron microscopy (TEM)

Myelin sheath thickness and axon morphology were evaluated in the regenerated nerves of implanted IC chitosan scaffolds and autograft groups using a transmission electron microscope (TEM, HITACHI H-7650). Collected nerve tissues were washed with PBS and fixed overnight in 2.5 % glutaraldehyde in 0.1 M cacodylate buffer at 4 °C, followed by washing with the buffer. Samples were then fixed in 1 % osmium tetroxide for 2 h, washed again, and incubated in uranyl acetate for 1 h at room temperature. The midsection of the scaffolds was analyzed to evaluate the regenerated axons. After dehydration, samples were embedded using a Poly/Bed 812 kit (Polysciences Inc., Warrington, PA). Ultra-thin sections (50–70 nm) were cut with a diamond knife and examined under TEM. The G-ratio was calculated using the formula: $G\text{-ratio} = D_i/D_o$, where D_i is the inner axon diameter and D_o is the outer diameter of the fiber [79].

5.4.7. Histological analysis

After euthanasia, the right sciatic nerve was harvested, rinsed with PBS, and placed in 10 % neutral buffered formalin for overnight fixation at 4 °C. The tissues were washed with PBS, transferred to 70 % ethanol, and embedded in paraffin. Three samples ($n = 3$) were prepared, and the mid-region of the regenerated nerve (center of the conduit or autograft) was sectioned into approximately 5 μm thick slices for histological analysis. Standard staining protocols were followed for the sectioned slices from sham-operated and repaired nerves. **Staining and Immunohistochemistry:** Hematoxylin and eosin (H&E) staining [79], Luxol fast blue staining (LFB) for myelin [79], and immunohistochemical staining for blood vessels (CD31), Schwann cells (S100 β) [79], and neurofilaments (NF-200) [79] were performed on tissue sections to assess nerve regeneration, myelination, and angiogenesis.

5.5. Statistical analysis

All data were presented as mean \pm standard deviation (SD). Statistical analyses, including t-tests and one-way analysis of variance (ANOVA) followed by Tukey's multiple comparisons, were conducted to assess the significance of differences between treatment groups. A confidence level of 95 % ($\alpha = 0.05$) was considered statistically significant for all analyses. All calculations and analyses were performed using GraphPad Prism 10 (GraphPad Software, Inc., La Jolla, CA).

CRediT authorship contribution statement

Rosalie Bordett: Writing – review & editing, Methodology, Formal analysis, Data curation. **Sama Abdulmalik:** Writing – review & editing, Methodology, Formal analysis, Data curation. **Allen Zennifer:** Writing – review & editing, Methodology, Formal analysis, Data curation. **Suranji Wijekoon:** Writing – review & editing, Methodology, Formal analysis, Data curation. **Sai Sadhananth Srinivasan:** Methodology, Formal analysis. **Ergin Coskun:** Methodology. **Yeshavanth Kumar Banasavadi Siddegowda:** Writing – review & editing, Methodology, Formal analysis, Data curation. **Xiaojun Yu:** Formal analysis. **Sangamesh G. Kumbar:** Writing – review & editing, Supervision, Project administration, Methodology, Funding acquisition, Formal analysis, Data curation, Conceptualization.

Ethics approval and consent to participate

All animals were maintained and cared for according to methods approved by the Institutional Animal Care and Use Committee (IACUC) at the University of Connecticut (Approval No: AP-200813-1125) and at University of Nebraska Medical Center (Approval No: IACUC # 24-069-

01-FC).

Declaration of competing interest

Corresponding author Sangamesh G. Kumbar is an Associate Editor for Bioactive Materials and was not involved in the editorial review or the decision to publish this article. All authors declare that there are no competing interests.

Acknowledgements

Dr. Kumbar acknowledges the funding support provided by the National Institutes of Health (#R01NS134604, #R01EB034202, #R01AR078908, and #R01EB030060) and the U.S. Army Medical Research Acquisition Activity (USAMRAA) through the CDMRP Peer-Reviewed Medical Research Program (Award No. W81XWH2010321, PR230581, and HT94252410137). Dr. Kumbar also acknowledges the DoD support from BA230234 (Award No. HT94252410944).

Appendix A. Supplementary data

Supplementary data to this article can be found online at <https://doi.org/10.1016/j.bioactmat.2025.03.017>.

References

- [1] K. Brattain, ANALYSIS OF THE PERIPHERAL NERVE REPAIR MARKET IN THE UNITED STATES, Magellan Medical Technology Consultants, Inc., 2013.
- [2] A.M. Moore, M. MacEwan, K.B. Santosa, K.E. Chenard, W.Z. Ray, D.A. Hunter, S. E. Mackinnon, P.J. Johnson, Acellular nerve allografts in peripheral nerve regeneration: a comparative study, *Muscle Nerve* 44 (2) (2011) 221–234.
- [3] P. Chrzyszcz, K. Derbisz, K. Suszyński, J. Miodoński, R. Trybulska, J. Lewin-Kowalik, W. Marcol, Application of peripheral nerve conduits in clinical practice: a literature review, *Neurol. Neurochir. Pol.* 52 (4) (2018) 427–435.
- [4] O.S. Manoukian, J.T. Baker, S. Rudraiah, M.R. Arul, A.T. Vella, A.J. Domb, S. G. Kumbar, Functional polymeric nerve guidance conduits and drug delivery strategies for peripheral nerve repair and regeneration, *J. Contr. Release* 317 (2020) 78–95.
- [5] Y. Shapira, V. Sammons, J. Forden, G.F. Guo, A. Kipp, J. Gurgulis, T. Mishra, J.D. de Villiers Alant, R. Midha, Brief electrical stimulation promotes nerve regeneration following experimental in-continuity nerve injury, *Neurosurgery* 85 (1) (2019) 156–163.
- [6] K.C. Tseng, H. Li, A. Clark, L. Sundem, M. Zuscik, M. Noble, J. Elfar, 4-Aminopyridine promotes functional recovery and remyelination in acute peripheral nerve injury, *EMBO Mol. Med.* 8 (12) (2016) 1409–1420.
- [7] F. Boriani, N. Fazio, F. Bolognesi, F.A. Pedrini, C. Marchetti, N. Baldini, Noncellular modification of acellular nerve allografts for peripheral nerve reconstruction: a systematic critical review of the animal literature, *Worlds Neurosurg.* 122 (2019) 692–703.
- [8] B. Guo, P.X. Ma, Conducting polymers for tissue engineering, *Biomacromolecules* 19 (6) (2018) 1764–1782.
- [9] P. Novak, A.N. Kopitar, G. Vidmar, A. Ihan, M. Štefanič, Therapeutic electrical stimulation and immune status in healthy men, *Int. J. Rehabil. Res.* 41 (4) (2018) 349–357.
- [10] J.K. Treathan, I. Baumgart, E.N. Nicolai, B.A. Gosink, A.J. Asp, M.L. Settell, S. R. Polacinda, K. Malerick, S.K. Brodnick, W. Zeng, A truly injectable neural stimulation electrode made from an in-body curing polymer/metal composite, *bioRxiv* (2019) 584995.
- [11] A. Heller, Searching for new truths of nature and creating people-serving products through bio-electrochemistry: the brain interface, *Curr. Opin. Electrochem.* 12 (2018) 3–4.
- [12] M.E. Shy, Peripheral neuropathies caused by mutations in the myelin protein zero, *J. Neurol. Sci.* 242 (1–2) (2006) 55–66.
- [13] R. Sherratt, H. Bostock, T. Sears, Effects of 4-aminopyridine on normal and demyelinated mammalian nerve fibres, *Nature* 283 (5747) (1980) 570–572.
- [14] O.S. Manoukian, S. Rudraiah, M.R. Arul, J.M. Bartley, J.T. Baker, X. Yu, S. G. Kumbar, Biopolymer-nanotube nerve guidance conduit drug delivery for peripheral nerve regeneration: in vivo structural and functional assessment, *Bioact. Mater.* 6 (9) (2021) 2881–2893.
- [15] P. Konofaos, J.P.V. Halen, Nerve repair by means of tubulization: past, present, future, *J. Reconstr. Microsurg.* 29 (3) (2013/03).
- [16] C.R. Carvalho, R.L. Reis, J.M. Oliveira H.J. Chun, R.L. Reis, A. Motta, G. Khang (Eds.), *Bioinspired Biomaterials. Advances in Experimental Medicine and Biology*, Springer, Singapore, 2020. https://doi.org/10.1007/978-981-15-3258-0_12, 1249.
- [17] S. Elyahoodayan, C. Larson, A.M. Cobo, E. Meng, D. Song, Acute in vivo testing of a polymer cuff electrode with integrated microfluidic channels for stimulation, recording, and drug delivery on rat sciatic nerve, *J. Neurosci. Methods* 336 (2020) 108634.

- [18] A. Aravamudhan, D.M. Ramos, A.A. Nada, S.G. Kumbar, Natural and synthetic biomedical polymers. *Natural Polymers: Polysaccharides and Their Derivatives for Biomedical Applications*, Elsevier, Amsterdam, Netherlands, 2014, pp. 67–89.
- [19] R. James, R.K. Nagarale, V.K. Sachan, C. Badalucco, P.K. Bhattacharya, S. G. Kumbar, Synthesis and characterization of electrically conducting polymers for regenerative engineering applications: sulfonated ionic membranes, *Polym. Adv. Technol.* 25 (12) (2014) 1439–1445.
- [20] A.A. Nada, M.R. Arul, D.M. Ramos, Z. Kroneková, J. Mosnáček, S. Rudraiah, S. G. Kumbar, Bioactive polymeric formulations for wound healing, *Polym. Adv. Technol.* 29 (6) (2018) 1815–1825.
- [21] B. Ferrigno, R. Bordett, N. Duraisamy, J. Moskow, M.R. Arul, S. Rudraiah, S. P. Nukavarapu, A.T. Vella, S.G. Kumbar, Bioactive polymeric materials and electrical stimulation strategies for musculoskeletal tissue repair and regeneration, *Bioact. Mater.* 5 (3) (2020/09/01).
- [22] Sulfonated and sulfated chitosan derivatives for biomedical applications: a review, *Carbohydr. Polym.* 202 (2018/12/15).
- [23] O.S. Manoukian, M.R. Arul, S. Rudraiah, I. Kalajzic, S.G. Kumbar, Aligned microchannel polymer-nanotube composites for peripheral nerve regeneration: small molecule drug delivery, *J. Contr. Release* 296 (2019) 54–67.
- [24] O.S. Manoukian, S. Stratton, M.R. Arul, J. Moskow, N. Sardashti, X. Yu, S. Rudraiah, S.G. Kumbar, Polymeric ionically conductive composite matrices and electrical stimulation strategies for nerve regeneration: in vitro characterization, *J. Biomed. Mater. Res. B Appl. Biomater.* 107 (6) (2019) 1792–1805.
- [25] O.S. Manoukian, S. Stratton, M.R. Arul, J. Moskow, N. Sardashti, X. Yu, S. Rudraiah, S.G. Kumbar, Polymeric ionically conductive composite matrices and electrical stimulation strategies for nerve regeneration: in vitro characterization, *J. Biomed. Mater. Res. B Appl. Biomater.* 107 (6) (2019/08/01).
- [26] R. James, R.K. Nagarale, V.K. Sachan, C. Badalucco, P.K. Bhattacharya, S. G. Kumbar, Synthesis and characterization of electrically conducting polymers for regenerative engineering applications: sulfonated ionic membranes, *Polym. Adv. Technol.* 25 (12) (2014/12/01).
- [27] Y. Zhu, C. Song, D. Yao, F. Qiao, Y. Zou, Y. Lv, Liquid metal-based conductive nerve guidance conduit combined with electrical stimulation boosts peripheral nerve repair, *J. Biomed. Mater. Res.* 113 (2) (2025/02/01).
- [28] S. Yin, J. Zhou, J. Wang, B. Xia, G. Chen, J.Z. Shiyun Yin, Jinsong Wang, Bin Xia, Guobao Chen, Preparation and performance of electrically conductive decellularized nerve matrix hydrogel conduits, *J. Biomater. Appl.* 38 (4) (2023-09-05).
- [29] M. Wang, P.-L. Tremblay, T. Zhang, Optimizing the electrical conductivity of polyacrylonitrile/polyaniline with nickel nanoparticles for the enhanced electrostimulation of Schwann cells proliferation, *Bioelectrochemistry* 140 (2021/08/01).
- [30] O.S. Manoukian, C. Marin, A. Ahmad, R. James, S.G. Kumbar, Biodegradable injectable implants for long-term delivery of contraceptives and other therapeutics, in: *IEEE Conference Publication | IEEE Xplore*, 2015 41st Annual Northeast Biomedical Engineering Conference (NEBEC), 2015.
- [31] S.P. Nichols, A. Koh, W.L. Storm, J.H. Shin, M.H. Schoenfish, *Biocompatible Materials for Continuous Glucose Monitoring Devices*, February 7, 2013.
- [32] R. Li, D.-h. Li, H.-y. Zhang, J. Wang, X.-k. Li, J. Xiao, R. Li, D.-h. Li, H.-y. Zhang, J. Wang, X.-k. Li, J. Xiao, Growth factors-based therapeutic strategies and their underlying signaling mechanisms for peripheral nerve regeneration, *Acta Pharmacol. Sin.* 41 (10) (2020), 41(10) (2020-20203-02).
- [33] V. Vukojevic, P. Mastrandreas, A. Arnold, F. Peter, I.-T. Kolassa, S. Wilker, T. Elbert, D.J.-F. de Quervain, A. Papassotiropoulos, A. Stetak, V. Vukojevic, P. Mastrandreas, A. Arnold, F. Peter, I.-T. Kolassa, S. Wilker, T. Elbert, D.J.-F. de Quervain, A. Papassotiropoulos, A. Stetak, Evolutionary conserved role of neural cell adhesion molecule-1 in memory, *Transl. Psychiatry* 10 (1) (2020), 10(1) (2020-07-06).
- [34] N. Li, S.-W. Teng, L. Zhao, J.-R. Li, J.-L. Xu, N. Li, J.-C. Shuai, Z.-Y. Chen, Carboxypeptidase E regulates activity-dependent TrkB neuronal surface insertion and hippocampal memory, *J. Neurosci.* 41 (33) (2021-08-18).
- [35] J.W. Russell, H.-L. Cheng, D. Golovoy, Insulin-like growth factor-I promotes myelination of peripheral sensory axons, *J. Neuropathol. Exp. Neurol.* 59 (7) (2000/07/01).
- [36] M. Chen, J. Zhao, X. Cai, S. Zhu, *Frontiers | Editorial: growth factors and stem cells intervention in injury repair and regeneration of spinal cord and peripheral nerve*, *Front. Pharmacol.* 13 (2023/01/09).
- [37] O.S. Manoukian, S. Rudraiah, M.R. Arul, J.M. Bartley, J.T. Baker, X. Yu, S. G. Kumbar, Biopolymer-nanotube nerve guidance conduit drug delivery for peripheral nerve regeneration: in vivo structural and functional assessment, *Bioact. Mater.* 6 (9) (2021) 2881–2893.
- [38] J.M. Cosgaya, J.R. Chan, E.M. Shooter, The neurotrophin receptor p75NTR as a positive modulator of myelination, *Science* 298 (5596) (2002) 1245–1248.
- [39] A. Rupp, U. Dornseifer, A. Fischer, W. Schmahl, K. Rodenacker, U. Jütting, P. Gais, E. Biemer, N. Papadopoulos, K. Matiassek, Electrophysiological assessment of sciatic nerve regeneration in the rat: surrounding limb muscles feature strongly in recordings from the gastrocnemius muscle, *J. Neurosci. Methods* 166 (2) (2007) 266–277.
- [40] S.W. Kemp, A.A. Webb, S. Dhaliwal, S. Syed, S.K. Walsh, R. Midha, Dose and duration of nerve growth factor (NGF) administration determine the extent of behavioral recovery following peripheral nerve injury in the rat, *Exp. Neurol.* 229 (2) (2011) 460–470.
- [41] E. Vogelin, J.M. Baker, J. Gates, V. Dixit, M.A. Constantinescu, N.F. Jones, Effects of local continuous release of brain derived neurotrophic factor (BDNF) on peripheral nerve regeneration in a rat model, *Exp. Neurol.* 199 (2) (2006) 348–353.
- [42] M. Anderson, N.B. Shelke, O.S. Manoukian, X. Yu, L.D. McCullough, S.G. Kumbar, Peripheral nerve regeneration strategies: electrically stimulating polymer based nerve growth conduits, *Crit. Rev. Biomed. Eng.* 43 (2–3) (2015) 131–159.
- [43] B. Hood, H.B. Levene, A.D. Levi, Transplantation of autologous Schwann cells for the repair of segmental peripheral nerve defects, *Neurosurg. Focus* 26 (2) (2009) E4.
- [44] M. Saheb-Al-Zamani, Y. Yan, S.J. Farber, D.A. Hunter, P. Newton, M.D. Wood, S. A. Stewart, P.J. Johnson, S.E. Mackinnon, Limited regeneration in long acellular nerve allografts is associated with increased Schwann cell senescence, *Exp. Neurol.* 247 (2013) 165–177.
- [45] T. Kornfeld, P.M. Vogt, C. Radtke, Nerve grafting for peripheral nerve injuries with extended defect sizes, *Wien. Med. Wochenschr.* 169 (9) (1946) (2019) 240–240.
- [46] R. Balint, N.J. Cassidy, S.H. Cartmell, Conductive polymers: towards a smart biomaterial for tissue engineering, *Acta Biomater.* 10 (6) (2014/06/01).
- [47] Y.-t. Wang, X.-t. Meng, A review of the evidence to support electrical stimulation-induced vascularization in engineered tissue, *Regener. Therapy* 24 (2023/12/01).
- [48] H. Durgam, S. Sapp, C. Deister, Z. Khaing, E. Chang, S. Luebben, C.E. Schmidt, Novel degradable Co-polymers of polypyrrole support cell proliferation and enhance neurite out-growth with electrical stimulation, *J. Biomater. Sci. Polym. Ed.* 21 (10) (2010-1-1).
- [49] A. Ul Haq, L. Montaina, F. Pescosolido, F. Carotenuto, F. Trovalusci, F. De Matteis, E. Tamburri, P. Di Nardo, A. Ul Haq, L. Montaina, F. Pescosolido, F. Carotenuto, F. Trovalusci, F. De Matteis, E. Tamburri, P. Di Nardo, Electrically conductive scaffolds mimicking the hierarchical structure of cardiac myofibers, *Sci. Rep.* 13 (1) (2023), 13(1) (2023-02-17).
- [50] H. Pang, L. Xu, D.-X. Yan, Z.-M. Li, Conductive polymer composites with segregated structures, *Prog. Polym. Sci.* 39 (11) (2014/11/01).
- [51] M. Anderson, N.B. Shelke, O.S. Manoukian, X. Yu, L.D. McCullough, S.G. Kumbar, Peripheral nerve regeneration strategies: electrically stimulating polymer based nerve growth conduits, *Crit. Rev. Biomed. Eng.* 43 (2–3) (2015).
- [52] Y. Qian, X. Zhao, Q. Han, W. Chen, H. Li, W. Yuan, Y. Qian, X. Zhao, Q. Han, W. Chen, H. Li, W. Yuan, An integrated multi-layer 3D-fabrication of PDA/RGD coated graphene loaded PCL nanoscaffold for peripheral nerve restoration, *Nat. Commun.* 9 (1) (2018), 9(1) (2018-01-22).
- [53] X. Li, W. Yang, H. Xie, J. Wang, L. Zhang, Z. Wang, L. Wang, CNT/Sericin conductive nerve guidance conduit promotes functional recovery of transected peripheral nerve injury in a rat model, *ACS Appl. Mater. Interfaces* 12 (33) (July 10, 2020).
- [54] Y. Lvov, W. Wang, L. Zhang, R. Fakhruddin, Halloysite clay nanotubes for loading and sustained release of functional compounds, *Adv. Mater.* 28 (6) (2016) 1227–1250.
- [55] L.R. Lizarraga-Valderrama, G. Ronchi, R. Nigmatullin, F. Fregnan, P. Basnett, A. Paxinou, S. Geuna, I. Roy, Preclinical study of peripheral nerve regeneration using nerve guidance conduits based on polyhydroxyalkanoates, *Bioeng. Transl. Med.* 6 (3) (2021/09).
- [56] A. Zennifer, S.K.P. Kumar, S. Bagewadi, S. Unnamalai, D. Chellappan, S. Abdulmalik, X. Yu, S. Sethuraman, D. Sundaramurthy, S.G. Kumbar, Innovative spiral nerve conduits: addressing nutrient transport and cellular activity for critical-sized nerve defects, *Bioact. Mater.* 44 (2025/02/01).
- [57] A star-PEG-heparin hydrogel platform to aid cell replacement therapies for neurodegenerative diseases, *Biomaterials* 30 (28) (2009/10/01).
- [58] Study on physical properties and nerve cell affinity of composite films from chitosan and gelatin solutions, *Biomaterials* 24 (17) (2003/08/01).
- [59] I. Kostadinova, N. Danchev, I. Kostadinova, N. Danchev, I. Kostadinova, N. Danchev, 4-aminopyridine – the new old drug for the treatment of neurodegenerative diseases, *Pharmacia* 66 (2) (2019/07/23).
- [60] A.R. Blight, J.P. Toombs, M.S. Bauer, W.R. Widmer, The Effects of 4-Aminopyridine on Neurological Deficits in Chronic Cases of Traumatic Spinal Cord Injury in Dogs: A Phase I Clinical Trial, vol. 8, 2009-03-26. <https://home.liebertpub.com/neu, 2>.
- [61] K.J. Smith, P.A. Felts, G.R. John, Effects of 4-aminopyridine on demyelinated axons, synapses and muscle tension, *Brain* 123 (1) (2000/01/01).
- [62] J.G. Yagüe, A. Cavaccini, A.C. Errington, V. Crunelli, G.D. Giovanni, Dopaminergic modulation of tonic but not phasic GABAA-receptor-mediated current in the ventral thalamus of Wistar and GAERS rats, *Exp. Neurol.* 247 (2013/09/01).
- [63] Z.C. Lateva, K.C. McGill, C.G. Bugar, Anatomical and electrophysiological determinants of the human thenar compound muscle action potential, *Muscle Nerve* 19 (11) (1996/11/01).
- [64] P.E. Barkhaus, S.D. Nandedkar, M.d. Carvalho, M. Swash, E.V. Stålberg, Revisiting the compound muscle action potential (CMAP), *Clini. Neurophysiol. Pract.* 9 (2024/01/01).
- [65] R.L.d.N. Transmission of impulses through cranial motor nuclei, *J. Neurophysiol.* 2 (5) (1939 Sep 01).
- [66] R. Shi, W. Sun, Potassium channel blockers as an effective treatment to restore impulse conduction in injured axons, *Neurosci. Bull.* 27 (1) (2011) 36–44.
- [67] V.K. Gupta, Y. You, V.B. Gupta, A. Klistorner, S.L. Graham, TrkB receptor signalling: implications in neurodegenerative, psychiatric and proliferative disorders, *Int. J. Mol. Sci.* 14 (5) (2013) 10122–10142.
- [68] L. Juckett, T.M. Saffari, B. Ormseth, J.-L. Senger, A.M. Moore, The effect of electrical stimulation on nerve regeneration following peripheral nerve injury, *Biomolecules* 12 (12) (2022) 1856.
- [69] S. Abdulmalik, J. Gallo, J. Nip, S. Katebifar, M. Arul, A. Lebaschi, L.N. Munch, J. M. Bartly, S. Choudhary, I. Kalajzic, Y.K. Banasavadi-Siddegowda, S. P. Nukavarapu, S.G. Kumbar, Nanofiber matrix formulations for the delivery of Exendin-4 for tendon regeneration: in vitro and in vivo assessment, *Bioact. Mater.* 25 (2023) 42–60.

- [70] J.A. Harrill, W.R. Mundy, Quantitative assessment of neurite outgrowth in PC12 cells, *Methods Mol. Biol.* 758 (2011) 331–348.
- [71] B. Boulan, A. Beghin, C. Ravello, J.-C. Deloulme, S. Gory-Fauré, A. Andrieux, J. Brocard, E. Denarier, AutoNeurite: an ImageJ plugin for measurement and classification of neuritic extensions, *PLoS One* 15 (7) (Jul 16, 2020).
- [72] S. Abdulmalik, J. Gallo, J. Nip, S. Katebifar, M. Arul, A. Lebaschi, L.N. Munch, J. M. Bartly, S. Choudhary, I. Kalajzic, Y.K. Banasavadi-Siddegowda, S. P. Nukavarapu, S.G. Kumbar, Nanofiber matrix formulations for the delivery of Exendin-4 for tendon regeneration: in vitro and in vivo assessment, *Bioact. Mater.* 25 (2023/07/01).
- [73] J. Qin, L. Wang, Y. Sun, X. Sun, C. Wen, M. Shahmoradi, Y. Zhou, Concentrated growth factor increases Schwann cell proliferation and neurotrophic factor secretion and promotes functional nerve recovery in vivo, *Int. J. Mol. Med.* 37 (2) (2016-02-01).
- [74] T. Mahmood, P.-C. Yang, Western blot: technique, theory, and trouble shooting, *N. Am. J. Med. Sci.* 4 (9) (2012/09).
- [75] K. Ohgane, H. Yoshioka, Quantification of Gel Bands by an Image J Macro, *Band/Peak Quantification Tool*, 2019.
- [76] Y.-K. Zhou, Z. Liang, Y. Guo, H.-T. Zhang, K.-H. Wang, High glucose upregulates CYP24A1 expression which attenuates the ability of 1,25(OH)₂D₃ to increase NGF secretion in a rat Schwann cell line RSC96, *Mol. Cell. Endocrinol.* 404 (2015/03/15).
- [77] W.D. Au - Arnold, K.A. Au - Sheth, C.G. Au - Wier, J.T. Au - Kissel, A.H. Au - Burghes, S.J. Au - Kolb, Electrophysiological motor unit number estimation (MUNE) measuring compound muscle action potential (CMAP) in mouse hindlimb muscles, *JoVE J.* 103 (2015) e52899.
- [78] A. Zennifer, D.R. Chellappan, P. Chinnaswamy, A. Subramanian, D. Sundaramurthi, S. Sethuraman, A. Zennifer, D.R. Chellappan, P. Chinnaswamy, A. Subramanian, D. Sundaramurthi, S. Sethuraman, Efficacy of 3D printed anatomically equivalent thermoplastic polyurethane guide conduits in promoting the regeneration of critical-sized peripheral nerve defects, *Biofabrication* 16 (4) (2024-07-25).
- [79] O.S. Manoukian, S. Rudraiah, M.R. Arul, J.M. Bartley, J.T. Baker, X. Yu, S. G. Kumbar, Biopolymer-nanotube nerve guidance conduit drug delivery for peripheral nerve regeneration: in vivo structural and functional assessment, *Bioact. Mater.* 6 (9) (2021/09).
- [80] R. Piovesana, A. Faroni, M. Taggi, A. Matera, M. Soligo, R. Canipari, L. Manni, A. J. Reid, A.M. Tata, Muscarinic receptors modulate Nerve Growth Factor production in rat Schwann-like adipose-derived stem cells and in Schwann cells, *Sci. Rep.* 10 (1) (2020).
- [81] F. Xu, H. Wu, K. Zhang, P. Lv, L. Zheng, J. Zhao, Pro-neurogenic effects of andrographolide on RSC96 Schwann cells in vitro, *Mol. Med. Rep.* 14 (4) (2016/10).
- [82] A. Shalizi, M. Lehtinen, B. Gaudillière, N. Donovan, J. Han, Y. Konishi, A. Bonni, Characterization of a neurotrophin signaling mechanism that mediates neuron survival in a temporally specific pattern, *J. Neurosci.* 23 (19) (2003/08/08).
- [83] V. Zermeño, S. Espindola, E. Mendoza, E. Hernández-Echeagaray, Differential expression of neurotrophins in postnatal C57BL/6 mice striatum, *Int. J. Biol. Sci.* 5 (2) (2009).
- [84] L. Zhang, Y. Li, C.-Y. Guan, S. Tian, X.-D. Lv, J.-H. Li, X. Ma, H.-F. Xia, Therapeutic effect of human umbilical cord-derived mesenchymal stem cells on injured rat endometrium during its chronic phase, *Stem Cell Res. Ther.* 9 (2018).
- [85] K. Nemoto, S. Miyata, F. Nemoto, T. Yasumoto, U. Murai, H. Kageyama, M. Degawa, Gene expression of neurotrophins and their receptors in lead nitrate-induced rat liver hyperplasia, *Biochem. Biophys. Res. Commun.* 275 (2) (2000/08/28).
- [86] G. Sorci, G. Giovannini, F. Riuzzi, P. Bonifazi, T. Zelante, S. Zagarella, F. Bistoni, R. Donato, L. Romani, The danger signal S100B integrates pathogen- and danger-sensing pathways to restrain inflammation, *PLoS Pathog.* 7 (3) (2011/03).
- [87] Y. Jiang, J. Liang, R. Li, Y. Peng, J. Huang, L. Huang, Basic fibroblast growth factor accelerates myelin debris clearance through activating autophagy to facilitate early peripheral nerve regeneration, *J. Cell Mol. Med.* 25 (5) (2021/03).